Trifluoromethyl-substituted Asymmetric Non-fullerene Acceptors enable Non-halogenated Solvent-processed Indoor Organic Photovoltaics with an Efficiency of over 30%

Peddaboodi Gopikrishna,‡[a] Muhammad Ahsan Saeed,‡[b] SungHyun Hur,‡[c] Gyeong Min Lee[d] Huijeong Choi,[a] Jae Won Shim,[d,*] and BongSoo Kim,[a,c,e,*]

[a]Department of Chemistry, Ulsan National Institute of Science and Technology (UNIST), 50 UNIST-gil, Ulsan 44919, Republic of Korea.

[b]Institute of Materials Science of Barcelona (ICMAB-CSIC), Campus UAB, Bellaterra 08193, Spain

[c]Graduate School of Semiconductor Materials and Device Engineering, Ulsan National Institute of Science and Technology (UNIST), 50 UNIST-gil, Ulsan 44919, Republic of Korea.

[d]School of Electrical Engineering, Korea University, Seoul 02841, Republic of Korea.

[e]Graduate School of Carbon Neutrality, Ulsan National Institute of Science and Technology (UNIST), 50 UNIST-gil, Ulsan 44919, Republic of Korea.

Corresponding Authors:

*E-mail: bongsoo@unist.ac.kr and jwshim19@korea.ac.kr

Author Contributions

‡These authors contributed equally.

Experimental section

Materials and Methods

PM6 and Y6 were purchased from Brilliant Matters, Inc. 4-(trifluoromethyl)-1-indanone was purchased from Alfa Aesar. Isobutyl nitrite and 1*H*-indene-1,2(3*H*)-dione were purchased from Sigma-Aldrich. 2,3-diaminomaleonitrile was purchased from Acros Organics. 3,9-diundecyl-12,13-dihydro-[1,2,5]thiadiazolo[3,4-*e*]thieno[2",3":4',5']thieno[2',3':4,5]pyrrolo[3,2-*g*]thieno[2',3':4,5]thieno -[3,2-*b*]indole was purchased from SunaTech Inc. 9*H*-indeno[1,2-*b*]pyrazine-2,3-dicarbonitrile (IPC) was synthesized according to a previously reported method.[1] 12,13-bis(2-butyloctyl)-3,9-diundecyl-12,13-dihydro-[1,2,5]thiadiazolo[3,4-*e*]thieno[2",3":4',5']thieno[2',3':4,5]pyrrolo[3,2-*g*]thieno-[2',3':4,5]thieno[3,2-*b*]indole-2,10-dicarbaldehyde (CHO-BBO-CHO) was synthesized according to a previously reported method.[2] 2-(5,6-difluoro-3-oxo-2,3-dihydro-1*H*-inden-1-ylidene)malononitrile (IC2F) and 2-(5,6-dichloro-3-oxo-2,3-dihydro-1*H*-inden-1-ylidene)malononitrile (IC2Cl) were purchased from Aaron Pharmatech Ltd. All solvents were purchased from commercial sources and used without further purification, unless otherwise mentioned.

Instrumentation

^{1}H, ^{13}C, and ^{19}F nuclear magnetic resonance (NMR) spectra were obtained using an Agilent 400 MHz FT-NMR spectrometer and a Bruker 400 MHz FT-NMR spectrometer in $CDCl_3$, with tetramethylsilane as the internal standard. Mass spectrometry was performed using an Ultraflex III matrix-assisted laser desorption ionization mass spectrometer (MALDI-TOF-MS) and an AccuTOF 4G+ DART time-of-flight mass spectrometer. UV-visible absorption spectra of the *o*-xylene solutions and films were recorded using an Agilent 8453 UV-visible spectrophotometer. The film samples were spin-coated onto a glass substrate using an *o*-xylene solution. Cyclic voltammetry was conducted using a CorrTest electrochemical workstation in an anhydrous acetonitrile solution of 0.1 mol/L of tetrabutylammonium hexafluorophosphate (Bu_4NPF_6) with platinum electrodes as the counter and working electrodes and Ag/AgCl as the reference electrode. Ferrocene was used as the internal standard. The non-fullerene acceptor (NFA) films were drop-cast onto the platinum working electrode from a chloroform solution. The highest occupied molecular orbital (HOMO) and lowest unoccupied molecular orbital (LUMO) energy levels were calculated by substituting the oxidation (E_{ox}) and reduction (E_{re}) potentials of the samples in -(E_{ox}-E_{fc}+4.8) eV and -(E_{re}-E_{fc}+4.8) eV. The LUMO energy levels of PM6 were estimated from the

difference between the HOMO and the optical bandgap of PM6. Differential scanning calorimetry (DSC) measurements were performed on a TA-Instruments DSC Q200 at a scanning rate of 10 °C/min.

The surface morphologies of the photoactive layer films were recorded using a Dimension ICON (Bruker Nano Surface, MA, USA). Grazing-incidence wide-angle X-ray scattering (GIWAXS) measurements were conducted at the PLS-II 6D UNIST-PAL beamline of the Pohang Accelerator Laboratory (PAL) in the Republic of Korea. X-rays from the bending magnet were monochromated using Si(111) double crystals and focused at the detector position using a toroidal mirror. GIWAXS patterns were recorded using a 2D CCD detector (MX225-HS, Rayonix L.L.C., USA), and the X-ray irradiation time was 100 s, depending on the saturation level of the detector. The sample-to-detector distance was 240 mm.

Device Fabrication and Electrical Measurements

Indium tin oxide (ITO)-patterned glass substrates (sheet resistance:10–15 Ω/sq.) were sequentially cleaned in deionized (DI) water + detergent, DI water, acetone, and isopropyl alcohol for 20 min each, and dried with a nitrogen gun. A layer of zinc oxide (ZnO) was then deposited over the glass/ITO substrates, followed by annealing at 200 °C on a hot plate for 30 min in air. Subsequently, photoactive layers were deposited in a nitrogen-filled glove box under the following conditions: PM6:Y6 (1:1.2) with a total concentration of 16 mg/mL in chloroform + 0.5% 1-chloronaphthalene (CN) additive was stirred for 3 h at 50 °C. The active layer was then spin-coated at 3000 rpm for 30 s and annealed at 100 °C on a hot plate for 10 min. For the binary devices, PM6:IPC-BBO-IC2F (21 mg/mL), PM6:IPC-BBO-IC2F(22 mg/mL), PM6:IPC1CF3-BBO-IC2F (24 mg/mL), and PM6:IPC1CF3-BBO-IC2Cl (22 mg/mL) were blended in an equal weight ratio in *o*-xylene solvent and stirred at 80 °C for 12 h. For the PM6:Y6:IPC1CF3-BBO-IC2F (22 mg/mL) and PM6:Y6:IPC1CF3-BBO-IC2Cl ternary devices, the ratio of NFAs was optimized by maintaining a constant total concentration of the blend (detailed compositions are provided in **Table S1** and **S2**). The binary and ternary active layers were then deposited at a spin speed of 2000 rpm for 30 s and subsequently annealed at 130 °C for 10 min. Finally, layers of molybdenum oxide (MoO_x) (10 nm) and silver (150 nm) were deposited in a thermal evaporator at a rate of 0.8 and 1.0 Å/s, respectively, under high pressure (~10^{-7} Pa) with a shadow mask. The active area of the organic photovoltaics (OPVs) for each device was measured as ~0.045 cm^2. The active area of

the OPVs was redefined using an aperture with an open area of 0.045 cm^2 to block the photocurrent generated at the edges of the active area defined by the top electrode. The current density-voltage (*J-V*) characteristics under 1-sun illumination were measured using software (K730) and a controlled source meter (2401, Keithley Instruments, Cleveland, OH, USA) (McScience, Republic of Korea) with an outdoor irradiance of 100 mW/cm^2. Light-emitting diode (LED) lamps (McScience, Republic of Korea), halogen lamps (HL) (OSRAM ECO PRO CLASSIC 64543 A 240 V 46 W E27; OSRAM, Munich, Germany), and fluorescent lamps (FL) were used for the indoor illumination evaluation. A slidac voltage regulator (SD-1000; DSELECTRON, Republic of Korea) was used to regulate the light intensity of the indoor light sources. A high-precision spectroradiometer (PMD100D, THORLABS) was used to measure the irradiance under indoor light. The external quantum efficiency spectra of the OPVs were recorded using a spectral measurement system (K3100 IQX; McScience, Republic of Korea).

The charge carrier mobilities of the blends were characterized using the space-charge-limited current (SCLC) method. Hole- and electron-only devices were fabricated with device configurations of ITO/2PACz/photoactive layer/MoO_x/Ag and ITO/ZnO/photoactive layer/PDINO/Al, respectively. The *J-V* curves of the OPVs were recorded using a Keithley 2401 measurement source unit at room temperature in air in the dark, and the carrier mobilities were extracted using the SCLC equation.

Synthesis of Non-fullerene Acceptors

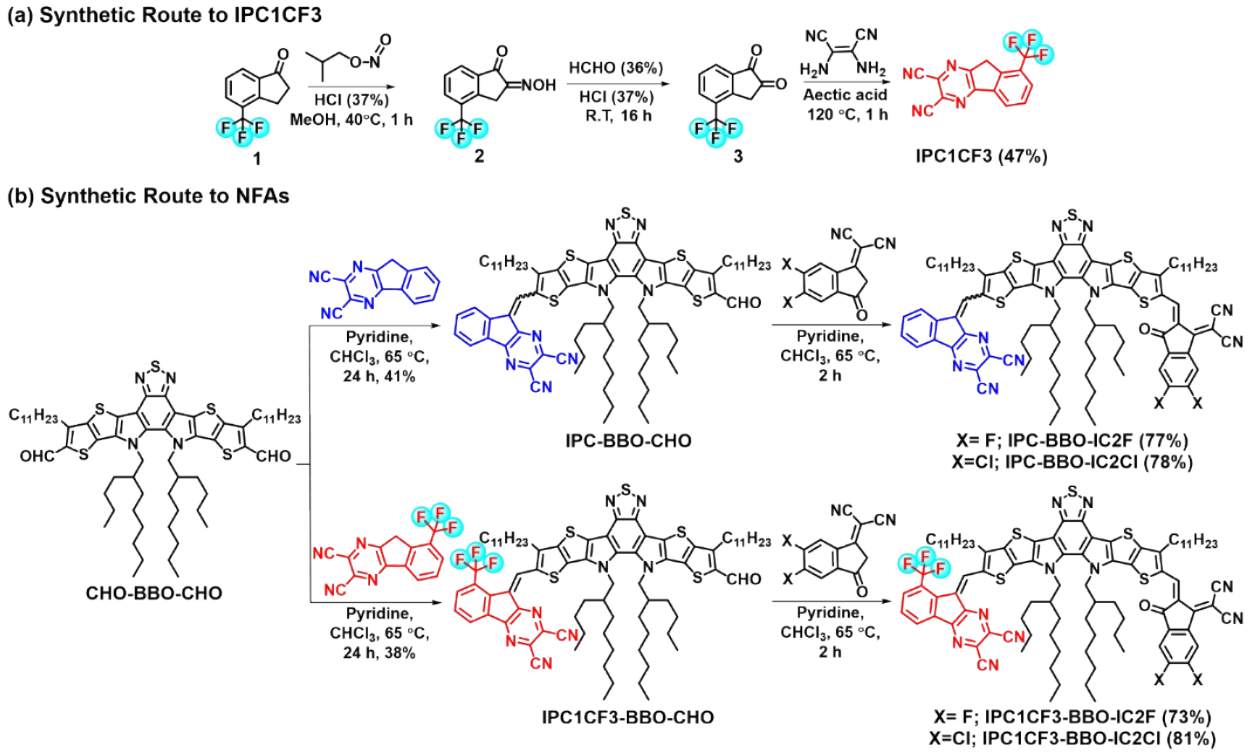

Scheme S1. The synthetic route of (a) IPC1CF3 and (b) NFAs.

Synthesis of (*Z*)-2-(hydroxyimino)-4-(trifluoromethyl)-2,3-dihydro-1*H*-inden-1-one (2):

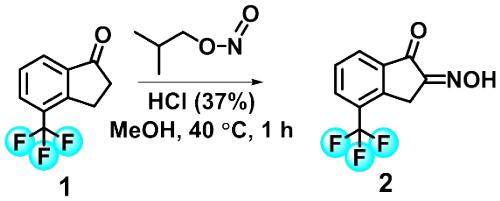

4-(trifluoromethyl)-1-indanone (1) (1000 mg, 4.99 mmol) was dissolved in methanol (15 mL) in a 50 mL round-bottom flask. 0.7 mL of concentrated hydrochloric acid (37%) was then added to a round-bottom flask, followed by the addition of isobutyl nitrite (772.70 mg, 7.49 mmol). The reaction mixture was stirred at 40 °C for 1 h under an argon atmosphere while monitoring the progress of the reaction using thin-layer chromatography (TLC). Upon completion of the reaction, the resulting mixture was poured into ice water, forming a precipitate. The precipitate was collected by filtration and dried under vacuum. The crude product was directly used in the next step without further purification.

Synthesis of 4-(trifluoromethyl)-1*H*-indene-1,2(3*H*)-dione (3):

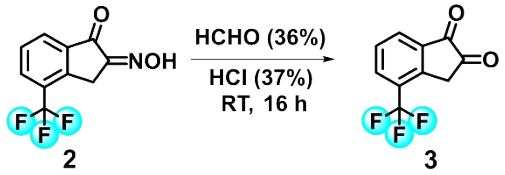

(*Z*)-2-(hydroxyimino)-4-(trifluoromethyl)-2,3-dihydro-1*H*-inden-1-one (2) (935 mg, 4.08 mmol) was suspended in 4 mL of formaldehyde (36%) and 8 mL of concentrated hydrochloric acid (37%). The resulting mixture was stirred at room temperature for 16 h. After completion of the reaction, the organic phase was extracted with ethyl acetate and washed with water. The organic phase was dried using anhydrous magnesium sulfate (Mg_2SO_4) and concentrated under vacuum. The crude product was used directly in the next step without any additional purification.

Synthesis of 8-(trifluoromethyl)-9*H*-indeno[1,2-*b*]pyrazine-2,3-dicarbonitrile (IPC1CF3):

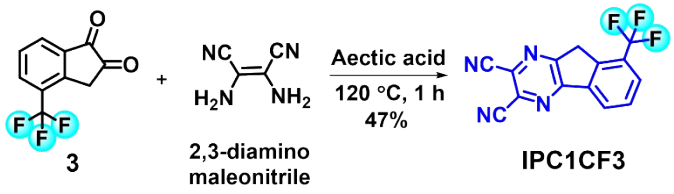

4-(trifluoromethyl)-1*H*-indene-1,2(3*H*)-dione (3) (815 mg, 3.80 mmol) and 2,3-diaminomaleonitrile (411.42 mg, 3.80 mmol) were dissolved in 35 mL of acetic acid. The reaction mixture was heated to 120 °C for 1 h. The reaction progress was monitored using TLC and once the reaction was complete, the reaction mixture was cooled to room temperature. The crude product was then extracted with ethyl acetate and washed with water. The organic phase was dried over $MgSO_4$ and concentrated under vacuum. The resulting crude product was purified using silica gel column chromatography using dichloromethane as the eluent. IPC1CF3 was obtained as a white solid (yield: 47%). ^{1}H NMR (400 MHz, $CDCl_3$) δ (ppm): 8.41 (d, *J*=8 Hz, 1H), 7.96 (d, *J*=8 Hz, 1H), 7.78 (t, 1H), 4.38 (s, 2H). ^{13}C NMR (100 MHz, $CDCl_3$) δ (ppm): 161.76, 155.80, 141.48, 137.02, 132.82, 130.59, 130.20, 130.16, 129.78, 127.50, 122.35, 113.76, 113.62, 35.87. ^{19}F NMR (376 MHz, $CDCl_3$) δ (ppm): -62.58 (s, 3F); HRMS (ESI): Calculated for $C_{14}H_5F_3N_4$ $[M + H]^+$: 287.0545, Found: 287.0540.

Synthesis of 9-((12,13-bis(2-butyloctyl)-10-formyl-3,9-diundecyl-12,13-dihydro-[1,2,5]thiadiazolo[3,4-*e*]thieno[2'',3'':4',5']thieno[2',3':4,5]pyrrolo[3,2-

***g*]thieno[2',3':4,5]thieno[3,2-*b*]indol-2-yl)methylene)-9*H*-indeno[1,2-*b*]pyrazine-2,3-dicarbonitrile (IPC-BBO-CHO):**

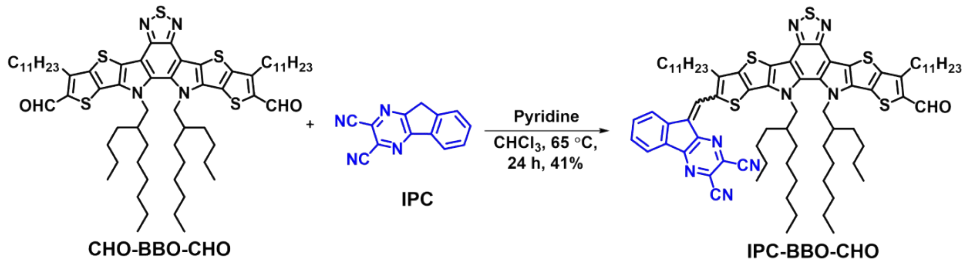

A mixture of CHO-BBO-CHO (1000 mg, 0.8773 mmol) and IPC (191.44 mg, 0.8773 mmol) was dissolved in 30 mL of chloroform. Next, 0.5 mL of pyridine was added, and the reaction mixture was stirred at 65 °C for 24 h. After the reaction was completed, the reaction mixture was cooled to room temperature and the chloroform was evaporated. The resulting crude product was purified using silica gel column chromatography with chloroform/hexane (4:1, v/v) as the eluent to obtain IPC-BBO-CHO as a dark green solid (yield: 41%). ^{1}H NMR (400 MHz, $CDCl_3$) δ (ppm): 10.15 (s, 1H), 8.98 & 8.25 (d, *J*=4 & *J*=4 Hz, 1H), 8.76 & 8.39 (s, 1H), 8.34 & 8.00 (d, *J*=4 & *J*=4 Hz, 1H), 7.79 & 7.75 (t, 1H), 7.68 & 7.58 (t, 1H), 4.75 & 4.67 (dd, 4H), 3.28-3.19 (m, 4H), 2.08 (m, 2H), 1.99-1.90 (m, 4H), 1.55-153 (m, 4H), 1.48-1.24 (m, 30H), 1.10-0.84 (m, 34H), 0.70-0.55 (m, 14H). ^{13}C NMR (100 MHz, $CDCl_3$) δ (ppm): 181.97, 153.20, 150.38, 147.69, 147.60, 146.93, 144.52, 144.24, 143.50, 143.08, 137.47, 134.14, 133.58, 133.13, 133.00, 132.15, 130.29, 129.91, 128.49, 128.37, 128.13, 127.90, 127.64, 123.90, 120.10, 119.33, 144.78, 114.66, 112.87, 112.80, 55.86, 55.62, 39.32, 39.16, 32.09, 31.73, 30.89, 30.66, 30.55, 30.34, 30.21, 29.98, 29.74, 29.59, 29.53, 28.37, 28.25, 28.16, 27.99, 25.57, 25.52, 25.43, 25.29, 25.23, 23.01, 22.96, 22.87, 22.67, 22.62, 14.32, 12.18, 14.11, 13.94. MS (MALDI-TOF): Calculated for $C_{79}H_{102}N_8OS_5$ $[M]^+$: 1338.678, Found: 1338.667.

Synthesis of 9-((12,13-bis(2-butyloctyl)-10-(((*Z*)-1-(dicyanomethylene)-5,6-difluoro-3-oxo-1,3-dihydro-2*H*-inden-2-ylidene)methyl)-3,9-diundecyl-12,13-dihydro-[1,2,5]thiadiazolo[3,4-*e*]thieno[2'',3'':4',5']thieno[2',3':4,5]pyrrolo[3,2-*g*]thieno[2',3':4,5]thieno[3,2-b]indol-2-yl)methylene)-9*H*-indeno[1,2-*b*]pyrazine-2,3-dicarbonitrile (IPC-BBO-IC2F):

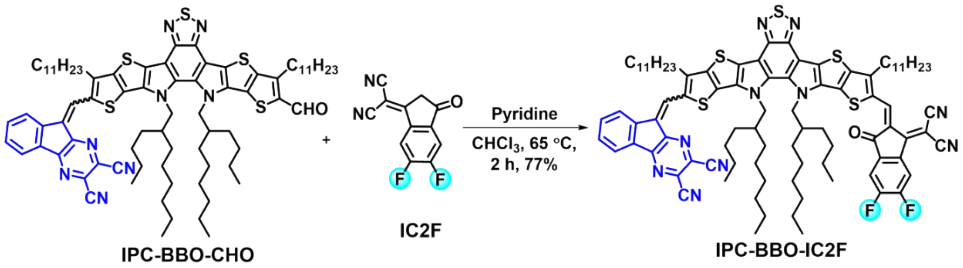

A mixture of IPC-BBO-CHO (300 mg, 0.2238 mmol) and IC2F (128.82 mg, 0.5596 mmol) was dissolved in 25 mL of chloroform. Next, 0.3 mL of pyridine was added, and the resulting mixture was heated to 65 °C for 2 h. After the reaction was completed, the reaction mixture was cooled to room temperature and the chloroform evaporated. The resulting crude product was purified using column chromatography on silica gel using chloroform/hexane (4:1, v/v) as the eluent to obtain dark blue IPC-BBO-IC2F as a solid (yield: 77%). ^{1}H NMR (400 MHz, $CDCl_3$) δ (ppm): 9.16 (s, 1H), 8.97 & 8.26 (d, *J*=4 & *J*=4 Hz, 1H), 8.76 & 8.40 (s, 1H), 8.59-8.55 (m, 1H), 8.35 & 8.01 (d, *J*=4 & *J*=4 Hz, 1H), 7.77-7.69 (m, 2H), 7.68 & 7.59 (tt, 1H), 4.81 & 4.75 (m, 4H), 3.29-3.23 (m, 4H), 2.16-2.09 (m, 2H), 1.99-1.85 (mm, 4H), 1.56-1.26 (m, 34H), 1.18-0.84 (m, 34H), 0.74-0.57 (m, 14H). ^{13}C NMR (100 MHz, $CDCl_3$) δ (ppm): 186.27, 159.16, 159.09, 156.21, 155.89, 155.76, 153.58, 153.28, 151.01, 150.66, 147.73, 136.84, 135.50, 135.04, 134.70, 133.12, 132.94, 131.40, 130.55, 128.61, 128.04, 124.05, 119.58, 115.27, 115.22, 114.99, 114.89, 114.77, 114.71, 113.90, 112.54, 68.48, 55.91, 39.60, 39.22, 32.12, 31.79, 31.46, 30.90, 30.78, 30.29, 30.16, 30.06, 29.99, 29.88, 29.84, 29.69, 29.56, 28.31, 28.03, 27.88, 25.81, 25.52, 25.37, 25.18, 23.06, 23.01, 22.91, 22.68, 14.34, 14.22, 14.17, 14.05, 14.00, 13.95. ^{19}F NMR (376 MHz, $CDCl_3$) δ (ppm): -123.13 & -123.30 (d, 1F), -124.45 & -124.52 (d, 1F). MS (MALDI-TOF): Calculated for $C_{91}H_{104}F_2N_{10}OS_5$ $[M]^+$: 1550.69, Found: 1550.719.

Synthesis of 9-((12,13-bis(2-butyloctyl)-10-(((*Z*)-5,6-dichloro-1-(dicyanomethylene)-3-oxo-1,3-dihydro-2*H*-inden-2-ylidene)methyl)-3,9-diundecyl-12,13-dihydro-[1,2,5]thiadiazolo[3,4-*e*]thieno[2'',3'':4',5']thieno[2',3':4,5]pyrrolo[3,2-*g*]thieno[2',3':4,5]thieno[3,2-*b*]indol-2-yl)methylene)-9*H*-indeno[1,2-*b*]pyrazine-2,3-dicarbonitrile (IPC-BBO-IC2Cl):

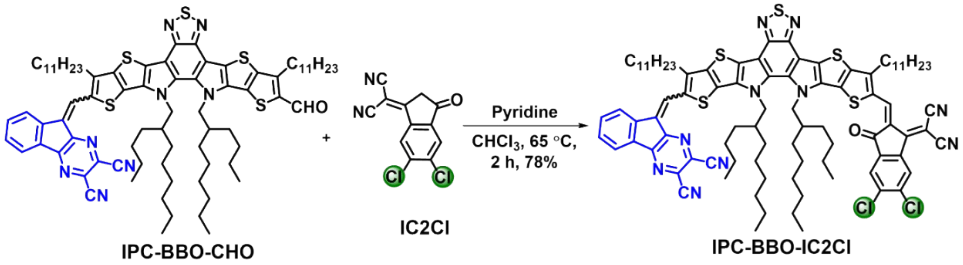

A mixture of IPC-BBO-CHO (300 mg, 0.2238 mmol) and IC2Cl (147.23 mg, 0.5596 mmol) was dissolved in 25 mL of chloroform. Next, 0.3 mL of pyridine was added, and the resulting mixture was heated to 65 °C for 2 h. After completion of the reaction, the reaction mixture was cooled to room temperature and the chloroform was evaporated. The resulting crude product was purified using column chromatography on silica gel using chloroform/hexane (4:1, v/v) as the eluent to obtain dark blue IPC-BBO-IC2Cl as a solid (yield: 78%). ^{1}H NMR (400 MHz, $CDCl_3$) δ (ppm): 9.19 (s, 1H), 8.97 & 8.26 (dd, *J*=8 Hz & *J*=8 Hz, 1H), 8.80 (s, 1H), 8.76 & 8.40 (s, 1H), 8.35 & 8.01 (dd, *J*=8 Hz & *J*=8 Hz, 1H), 7.97 (s, 1H), 7.76 (t, 1H), 7.71 & 7.60 (tt, 1H) 4.78-4.70 (m, 4H), 3.29-3.23 (m, 4H), 2.12 (m, 2H), 1.99-1.96 (m, 2H), 1.91-1.87 (m, 2H) 1.56-1.26 (m, 40H) 1.16-0.86 (m, 28H), 0.77-0.58 (m, 14H). ^{13}C NMR (100 MHz, $CDCl_3$) δ (ppm): 186.29, 158.93, 158.88, 153.52, 150.55, 147.75, 147.62, 145.36, 145.10, 144.78, 143.12, 139.53, 139.23, 138.92, 136.24, 135.90, 135.79, 135.20, 133.23, 133.11, 132.92, 132.77, 131.72, 130.52, 128.62, 128.49, 128.19, 128.06, 126.99, 125.10, 124.01, 119.68, 119.54, 115.35, 114.89, 114.71, 114.01, 133.90, 113.01, 68.40, 55.94, 39.63, 39.26, 32.12, 31.85, 31.78, 31.46, 30.91, 30.78, 30.48, 30.29, 30.18, 30.07, 30.01, 29.84, 29.70, 29.56, 29.09, 28.64, 28.53, 28.30, 28.04, 27.93, 25.93, 25.64, 25.55, 25.38, 25.24, 23.06, 23.01, 22.91, 22.69, 14.34, 14.26, 14.17, 14.07, 13.96. MS (MALDI-TOF): Calculated for $C_{91}H_{104}Cl_2N_{10}OS_5$ $[M]^+$: 1582.63, Found: 1582.636.

Synthesis of (*Z*)-9-((12,13-bis(2-butyloctyl)-10-formyl-3,9-diundecyl-12,13-dihydro-[1,2,5]thiadiazolo[3,4-*e*]thieno[2'',3'':4',5']thieno[2',3':4,5]pyrrolo[3,2-*g*]thieno[2',3':4,5]thieno[3,2-*b*]indol-2-yl)methylene)-8-(trifluoromethyl)-9*H*-indeno[1,2-*b*]pyrazine-2,3-dicarbonitrile (IPC1CF3-BBO-CHO):

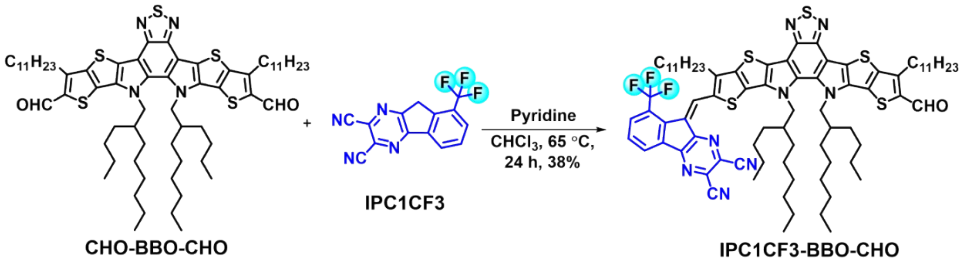

A mixture of CHO-BBO-CHO (1000 mg, 0.8773 mmol) and IPC1CF3 (251.09 mg, 0.8773 mmol) was dissolved in chloroform (30 mL). Next, pyridine (0.5 mL) was added, and the reaction mixture was stirred at 65 °C for 24 h. After the reaction was completed, the reaction mixture was cooled to room temperature and the chloroform evaporated. The resulting crude product was purified using silica gel column chromatography using chloroform/hexane (4:1, v/v) as the eluent to obtain IPC1CF3-BBO-CHO as a dark green solid (yield: 38%). ^{1}H NMR (400 MHz, $CDCl_3$) δ (ppm): 10.16 (s, 1H), 8.96 (s, 1H), 8.50 (d, *J*=8 Hz, 1H), 8.06 (d, *J*=8 Hz, 1H), 7.65 (t, 1H), 4.78 & 4.68 (dd, 4H), 3.26 & 3.20 (m, 4H), 2.10 (m, 2H), 1.96-1.91 (m, 4H), 1.56 (m, 4H), 1.48-1.26 (m, 30H), 1.10-0.85 (m, 34H), 0.68-0.58 (m, 14H). ^{13}C NMR (100 MHz, $CDCl_3$) δ (ppm): 181.98, 151.21, 150.46, 149.88, 147.77, 146.91, 144.56, 143.67, 139.79, 137.60, 137.51, 137.45, 135.89, 134.43, 134.20, 134.09, 132.97, 132.56, 130.92, 129.84, 129.16, 128.48, 127.93, 127.60, 127.31, 127.04, 117.89, 114.67, 114.33, 113.19, 112.87, 112.86, 55.99, 55.63, 39.31, 39.22, 32.12, 31.72, 31.59, 30.62, 30.56, 30.49, 30.37, 30.34, 30.26, 30.16, 30.10, 29.92, 29.85, 29.82, 29.80, 29.73, 29.71, 29.67, 29.60, 29.54, 29.51, 28.39, 28.23, 28.20, 28.09, 25.51, 25.48, 25.31, 22.98, 22.94, 22.90, 22.89, 22.69, 22.67, 22.62, 14.33, 14.32, 14.17, 14.16, 14.11, 13.96, 13.93. ^{19}F NMR (376 MHz, $CDCl_3$) δ (ppm): -59.70 (s, 3F). MS (MALDI-TOF): Calculated for $C_{80}H_{101}F_3N_8OS_5$ $[M]^+$: 1406.665, Found: 1406.706.

Synthesis of (*Z*)-9-((12,13-bis(2-butyloctyl)-10-(((*Z*)-1-(dicyanomethylene)-5,6-difluoro-3-oxo-1,3-dihydro-2*H*-inden-2-ylidene)methyl)-3,9-diundecyl-12,13-dihydro-[1,2,5]thiadiazolo[3,4-*e*]thieno[2'',3'':4',5']thieno[2',3':4,5]pyrrolo[3,2-*g*]thieno[2',3':4,5]thieno[3,2-b]indol-2-yl)methylene)-8-(trifluoromethyl)-9*H*-indeno[1,2-*b*]pyrazine-2,3-dicarbonitrile (IPC1CF3-BBO-IC2F):

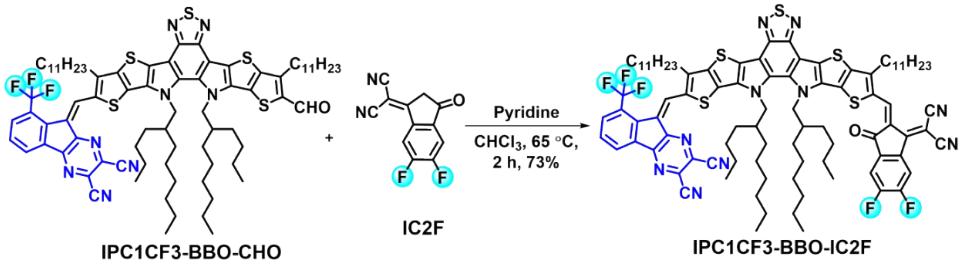

A mixture of IPC1CF3-BBO-CHO (300 mg, 0.1851 mmol) and IC2F (106.54 mg, 0.4629 mmol) was dissolved in 25 mL of chloroform. Next, 0.3 mL of pyridine was added, and the resulting mixture was heated to 65 °C for 2 h. After the reaction was completed, the reaction mixture was cooled to room temperature and the chloroform evaporated. The resulting crude product was purified using column chromatography on silica gel using chloroform/hexane (4:1, v/v) as the eluent to obtain dark blue IPC1CF3-BBO-IC2F as a solid (yield: 73%). ^{1}H NMR (400 MHz, $CDCl_3$) δ (ppm): 9.17 (s, 1H), 8.98 (s, 1H), 8.59-8.555 (m, 1H), 8.51 (d, *J*=8 Hz, 1H), 8.09 (d, *J*=8 Hz, 1H), 7.73-7.66 (m, 2H), 4.84-4.76 (m, 4H), 3.28-3.23 (m, 4H), 2.15-2.11 (m, 2H), 1.95-1.85 (m, 4H), 1.59-1.42 (m, 4H) 1.40- 1.26 (m, 30H), 1.18-0.82 (m, 36H), 0.74-0.58 (m, 14H). ^{13}C NMR (100 MHz, $CDCl_3$) δ (ppm): 186.27, 159.15, 155.93, 155.79, 154.09, 153.33, 153.18, 151.11, 150.71, 150.04, 147.79, 147.70, 145.19, 145.07, 139.80, 138.24, 137.67, 136.89, 136.77, 136.50, 135.89, 135.84, 135.50, 134.78, 134.61, 134.04, 133.42, 132.74, 131.23, 131.03, 130.96, 129.06, 128.56, 128.21, 127.42, 127.29, 124.07, 123.74, 119.99, 118.44, 115.25, 115.02, 114.87, 114.64, 114.37, 113.92, 113.31, 112.76, 112.57, 68.64, 55.99, 39.58, 39.28, 32.14, 31.79, 31.61, 31.47, 30.91, 30.78, 30.73, 30.32, 30.07, 29.94, 29.84, 29.73, 29.69, 29.57, 28.54, 28.30, 28.10, 27.95, 25.82, 25.57, 25.42, 25.26, 23.05, 22.91, 22.68, 14.34, 14.22, 14.16, 14.05, 13.97. ^{19}F NMR (376 MHz, $CDCl_3$) δ (ppm): -59.72 (s, 3F), -123.22 (d, 1F), -124.38 (d, 1F). MS (MALDI-TOF): Calculated for $C_{92}H_{103}F_5N_{10}OS_5$ $[M]^+$: 1618.684, Found: 1618.703.

Synthesis of (*Z*)-9-((12,13-bis(2-butyloctyl)-10-(((*Z*)-5,6-dichloro-1-(dicyanomethylene)-3-oxo-1,3-dihydro-2*H*-inden-2-ylidene)methyl)-3,9-diundecyl-12,13-dihydro-[1,2,5]thiadiazolo[3,4-*e*]thieno[2'',3'':4',5']thieno[2',3':4,5]pyrrolo[3,2-*g*]thieno[2',3':4,5]thieno[3,2-*b*]indol-2-yl)methylene)-8-(trifluoromethyl)-9*H*-indeno[1,2-*b*]pyrazine-2,3-dicarbonitrile (IPC1CF3-BBO-IC2Cl):

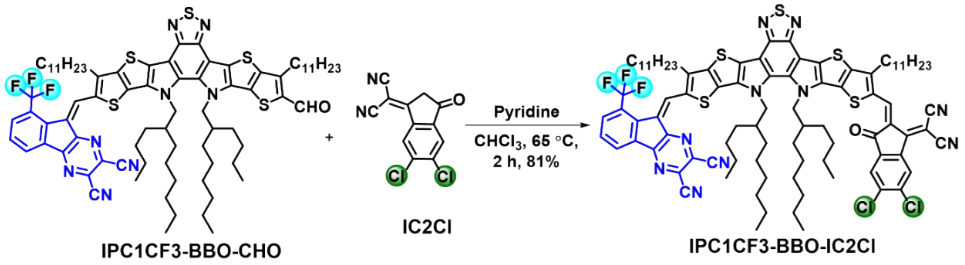

A mixture of IPC1CF3-BBO-CHO (300 mg, 0.1814 mmol) and IC2Cl (119.35 mg, 0.4536 mmol) was dissolved in 25 mL of chloroform. Next, 0.3 mL of pyridine was added, and the resulting mixture was heated to 65 °C for 2 h. After completion of the reaction, the reaction mixture was cooled to room temperature and the chloroform was evaporated. The resulting crude product was purified using column chromatography on silica gel using chloroform/hexane (4:1, v/v) as the eluent to obtain dark blue IPC1CF3-BBO-IC2Cl as a solid (yield: 81%). ^{1}H NMR (400 MHz, $CDCl_3$) δ (ppm): 9.17 (s, 1H), 8.96 (s, 1H), 8.78 (s, 1H), 8.52 (d, *J*=8 Hz, 1H), 8.08 (d, *J*=8 Hz, 1H), 7.96 (s, 1H), 7.67 (t, 1H), 4.84-4.77 (m, 4H), 3.26-3.23 (m, 4H), 2.17-2.12 (m, 2H), 1.92-1.89 (m, 4H), 1.52-1.48 (m, 4H) 1.44-1.26 (m, 30H), 1.18-0.81 (m, 34H), 0.73-0.58 (m, 14H). ^{13}C NMR (100 MHz, $CDCl_3$) δ (ppm): 186.35, 159.02, 154.32, 151.01, 150.72, 150.03, 147.80, 147.69, 145.31, 145.12, 139.79, 139.63, 139.33, 138.97, 138.31, 137.66, 136.85, 136.31, 136.00, 135.87, 135.81, 134.93, 134.64, 134.03, 133.77, 133.36, 132.75, 131.51, 131.11, 130.96, 129.06, 128.58, 128.23, 127.53, 127.42, 127.30, 127.07, 125.18, 119.92, 118.47, 115.35, 114.87, 114.62, 114.36, 114.02, 113.31, 110.26, 106.99, 68.62, 56.06, 39.59, 39.30, 32.13, 31.79, 31.60, 31.47, 30.90, 30.78, 30.34, 30.21, 30.08, 29.84, 29.73, 29.68, 29.57, 28.48, 28.27, 28.10, 28.00, 25.90, 25.65, 25.42, 25.29, 23.03, 22.96, 22.91, 22.68, 14.33, 14.25, 14.16, 14.03, 13.97. ^{19}F NMR (376 MHz, $CDCl_3$) δ (ppm): -59.73 (s, 3F). MS (MALDI-TOF): Calculated for $C_{92}H_{103}Cl_2F_3N_{10}OS_5$ $[M]^+$: 1650.624, Found: 1650.804.

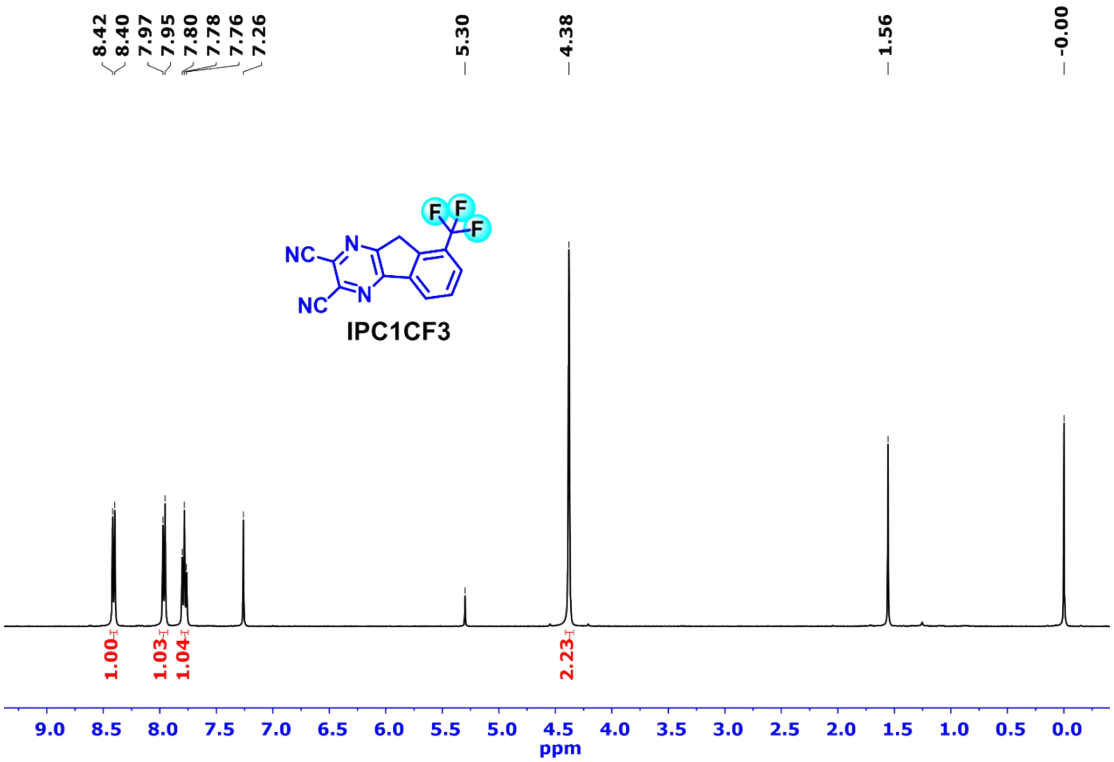

Fig. S1 ^{1}H NMR spectrum of IPC1CF3 in $CDCl_3$.

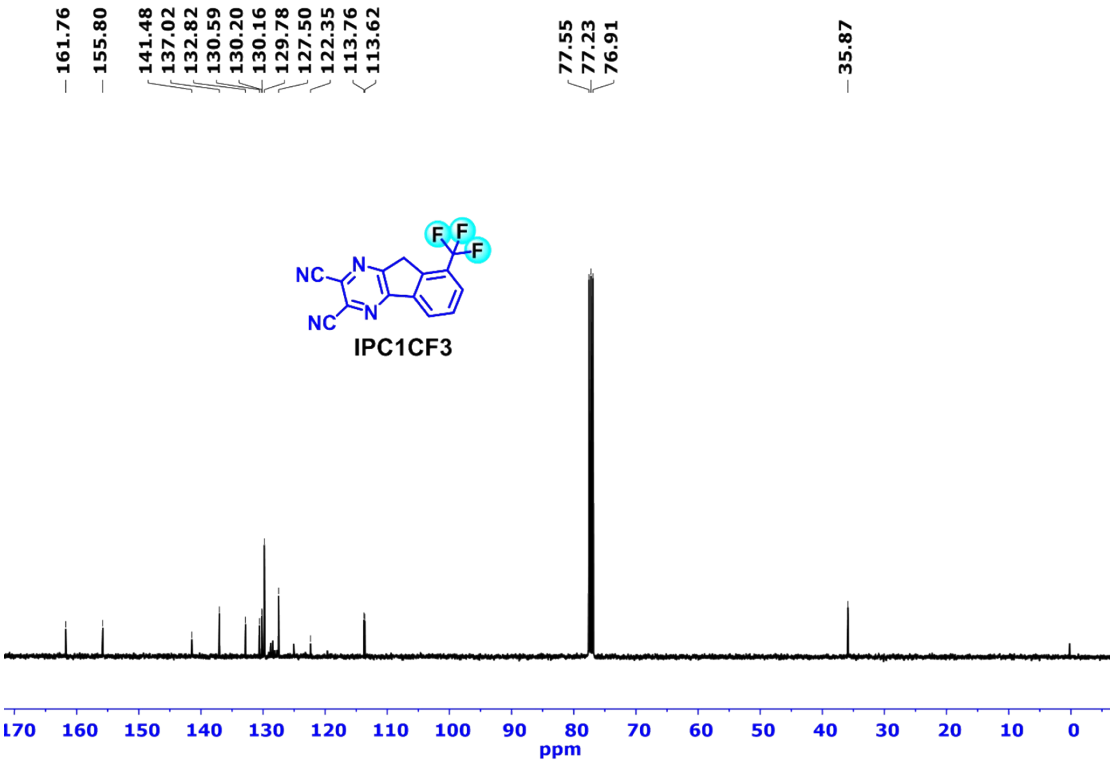

Fig. S2 ^{13}C NMR spectrum of IPC1CF3 in $CDCl_3$.

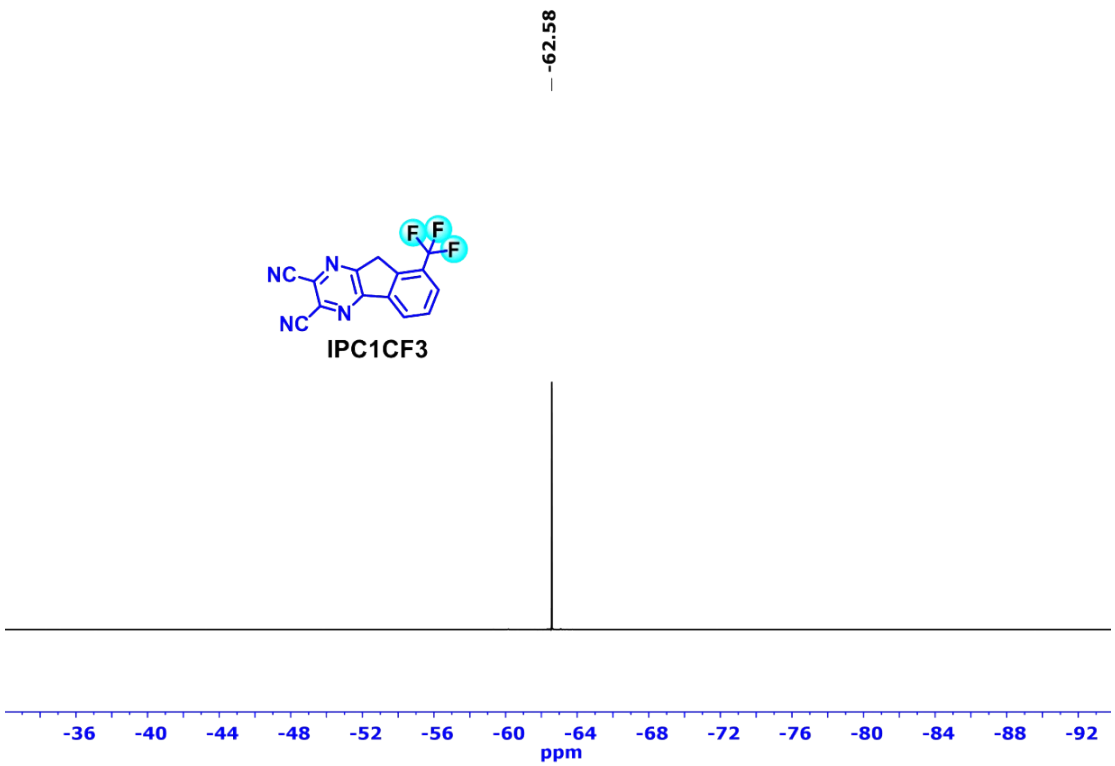

Fig. S3 ^{19}F NMR spectrum of IPC1CF3 in $CDCl_3$.

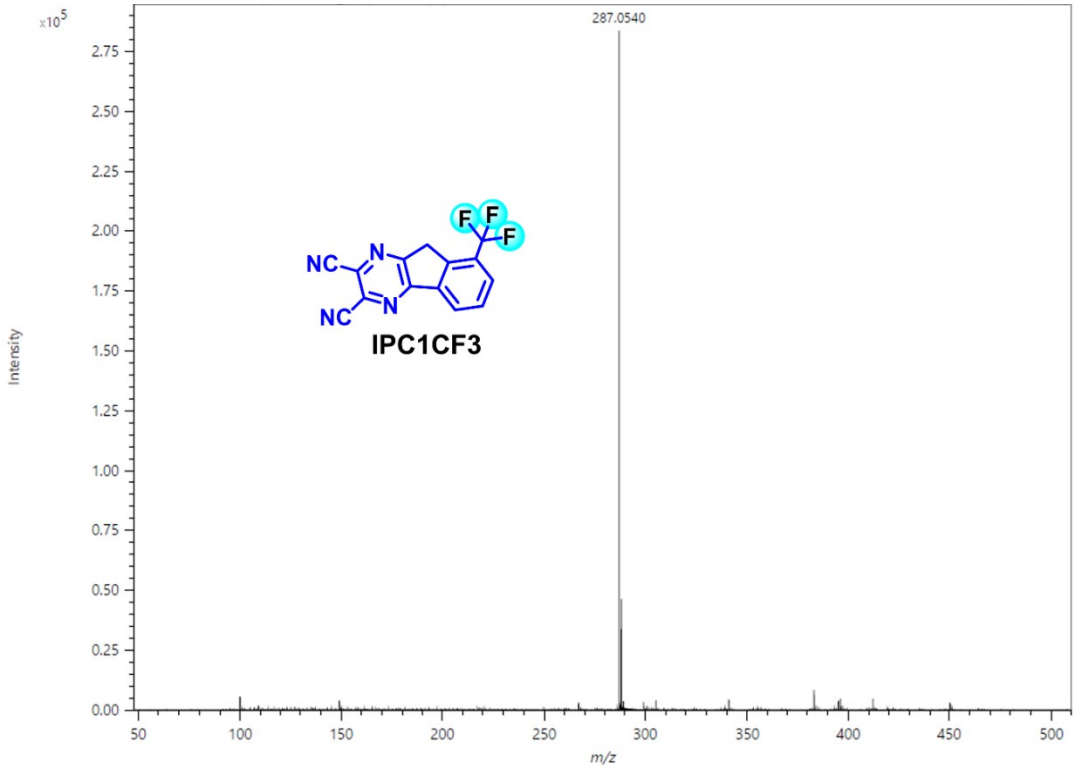

Fig. S4 HRMS spectrum of IPC1CF3.

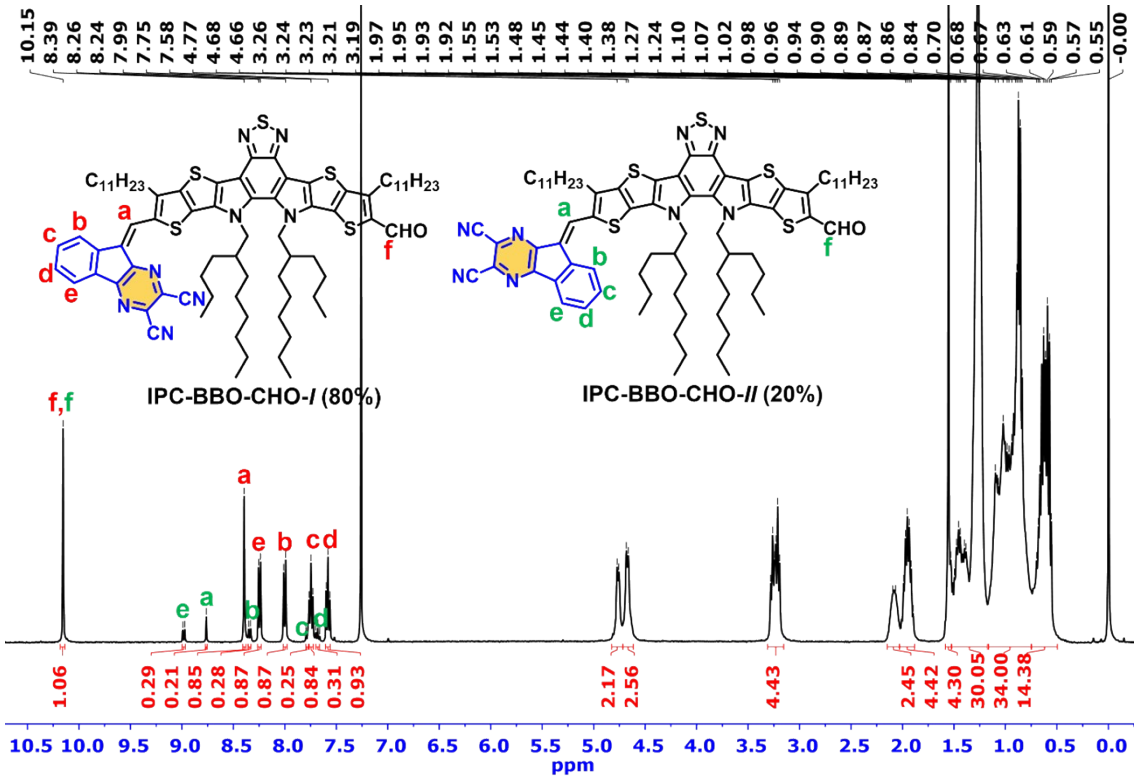

Fig. S5 ^{1}H NMR spectrum of IPC-BBO-CHO in $CDCl_3$.

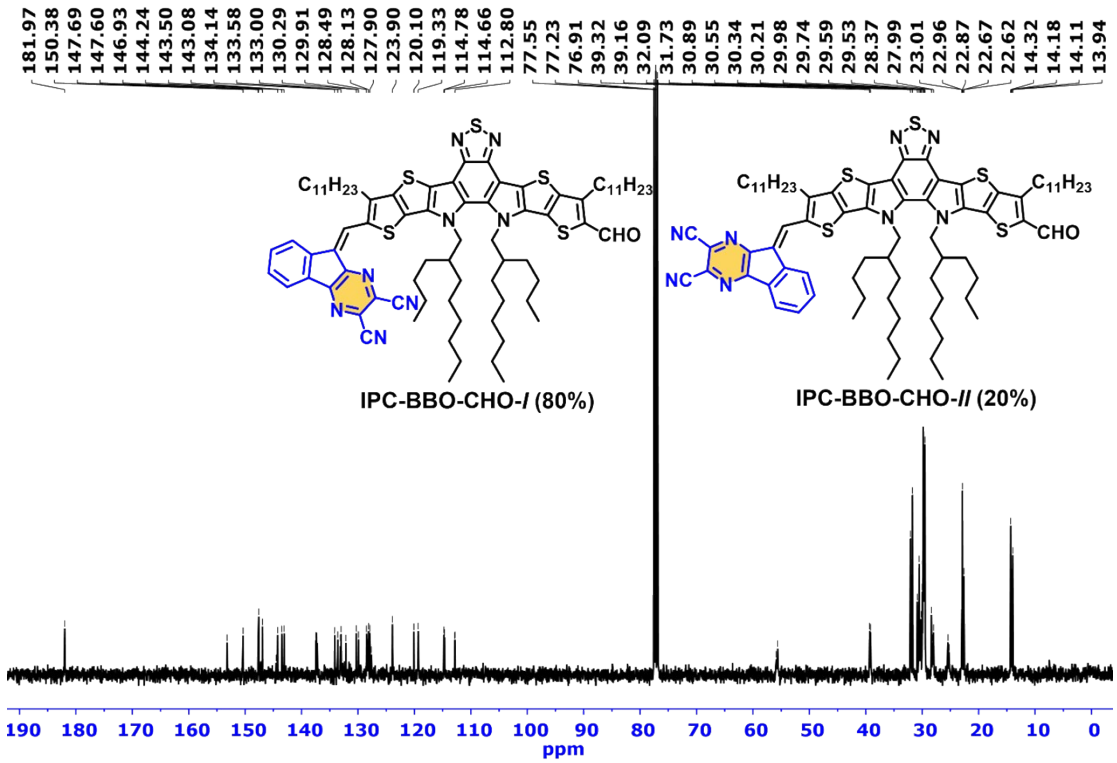

Fig. S6 ^{13}C NMR spectrum of IPC-BBO-CHO in $CDCl_3$.

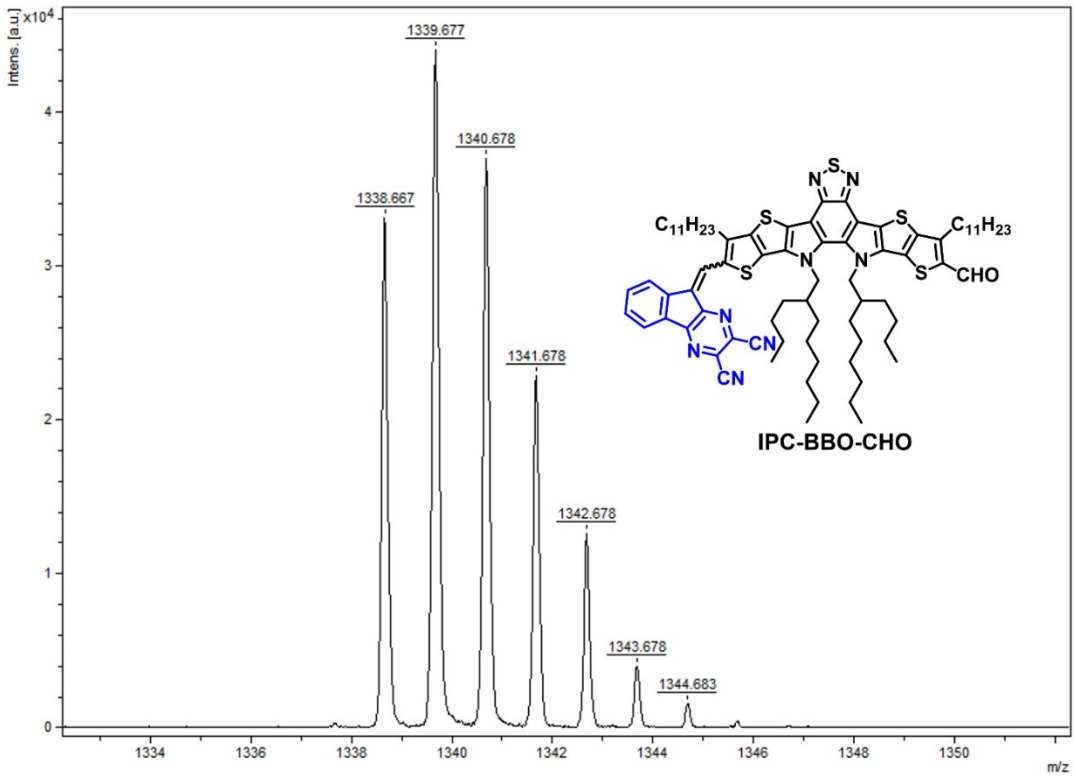

Fig. S7 Mass spectrum of IPC-BBO-CHO by MALDI-TOF.

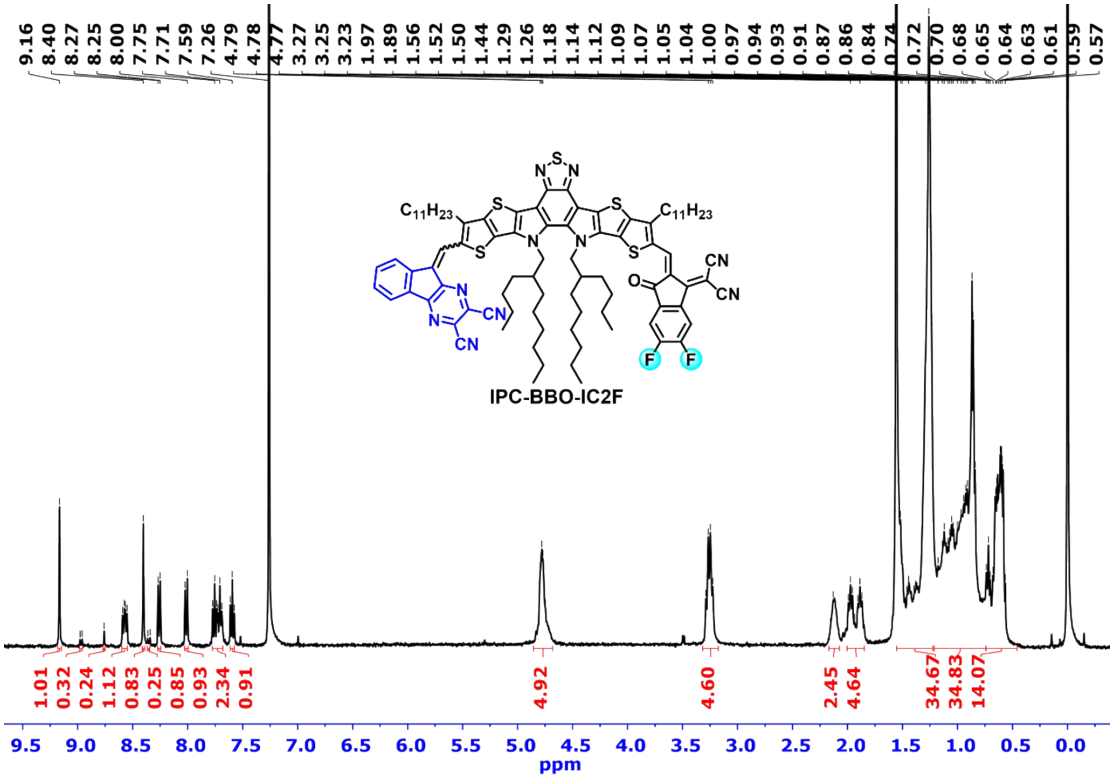

Fig. S8 ^{1}H NMR spectrum of IPC-BBO-IC2F in $CDCl_3$.

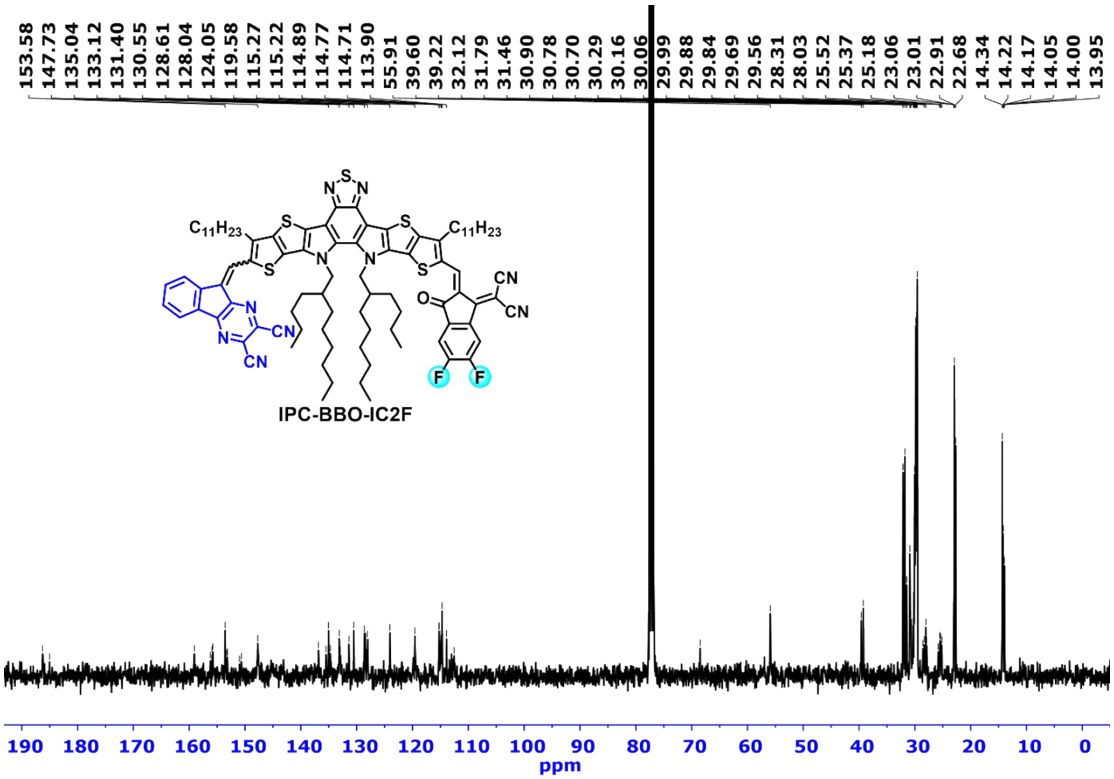

Fig. S9 ^{13}C NMR spectrum of IPC-BBO-IC2F in $CDCl_3$.

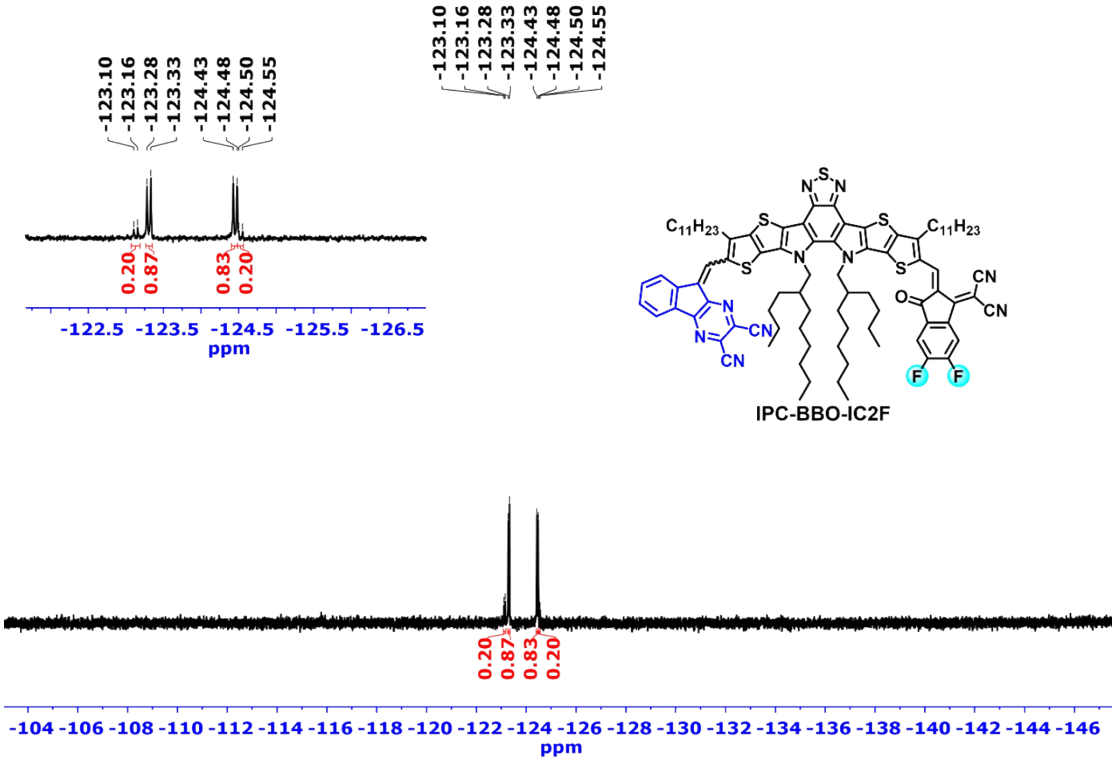

Fig. S10 ^{19}F NMR spectrum of IPC-BBO-IC2F in $CDCl_3$.

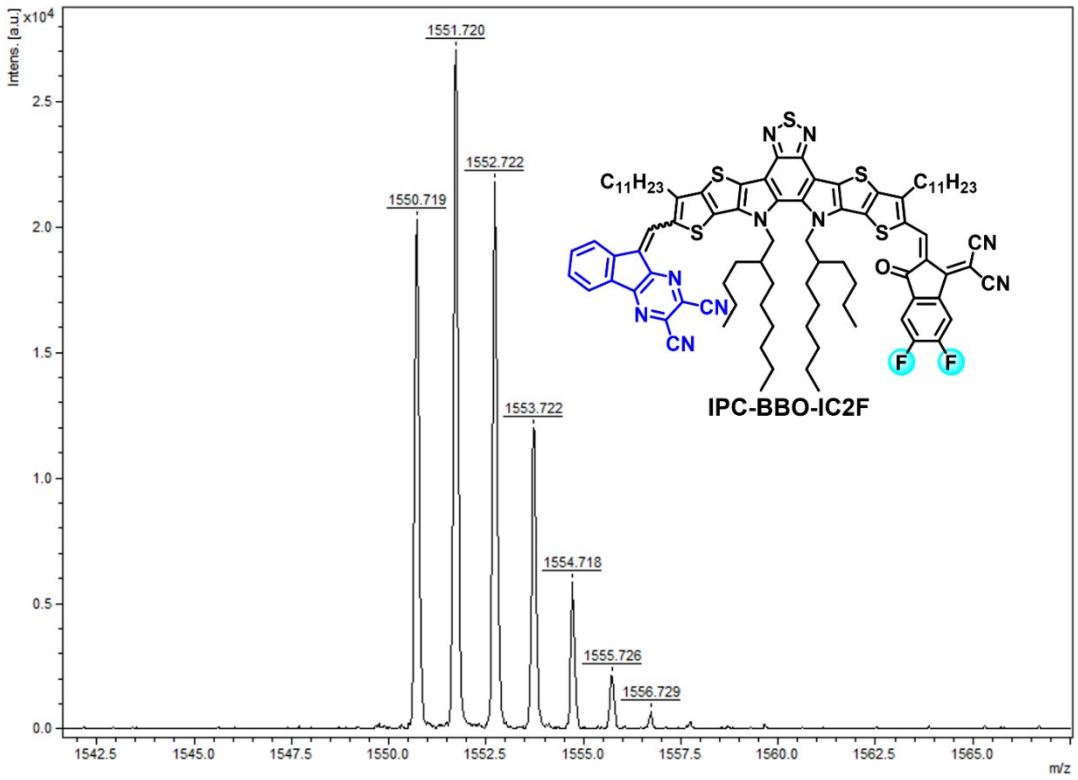

Fig. S11 Mass spectrum of IPC-BBO-IC2F by MALDI-TOF.

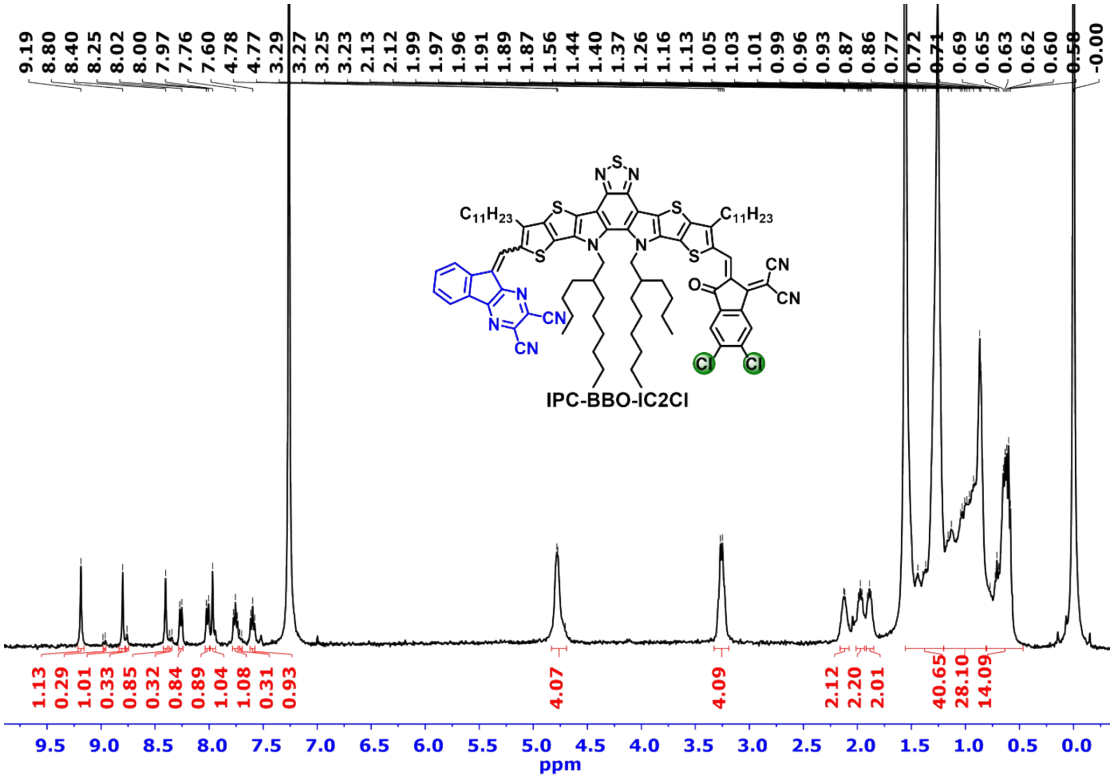

Fig. S12 ^{1}H NMR spectrum of IPC-BBO-IC2Cl in $CDCl_3$.

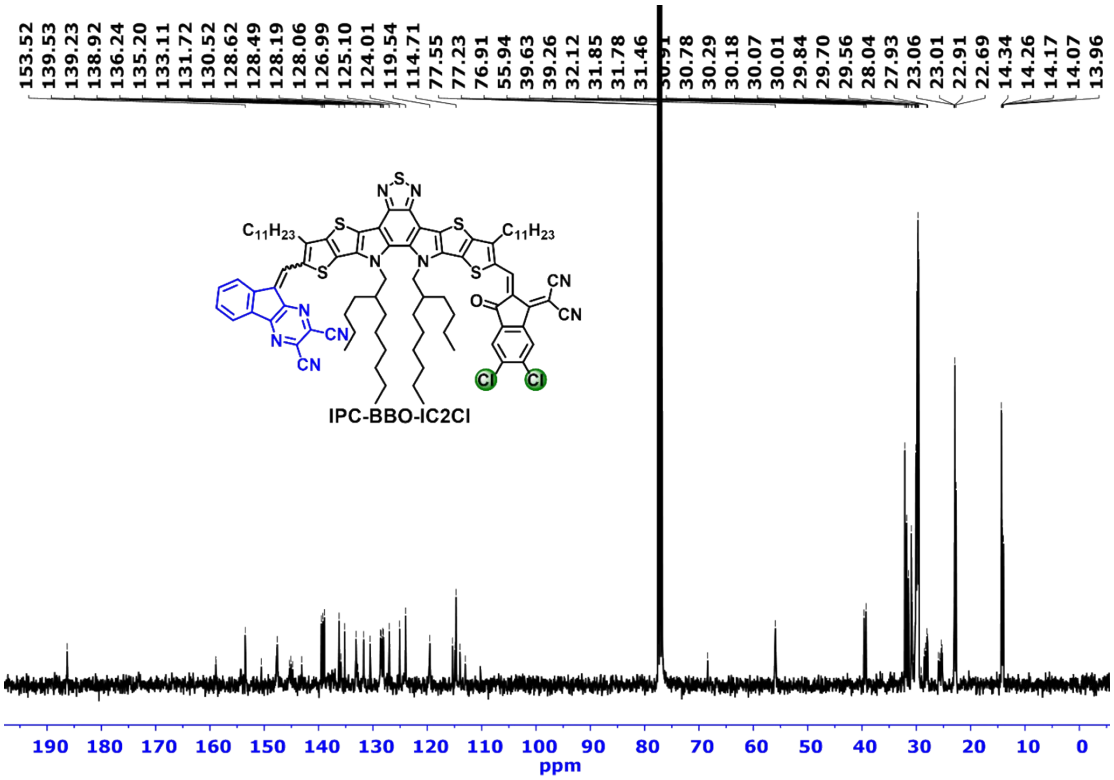

Fig. S13 ^{13}C NMR spectrum of IPC-BBO-IC2Cl in $CDCl_3$.

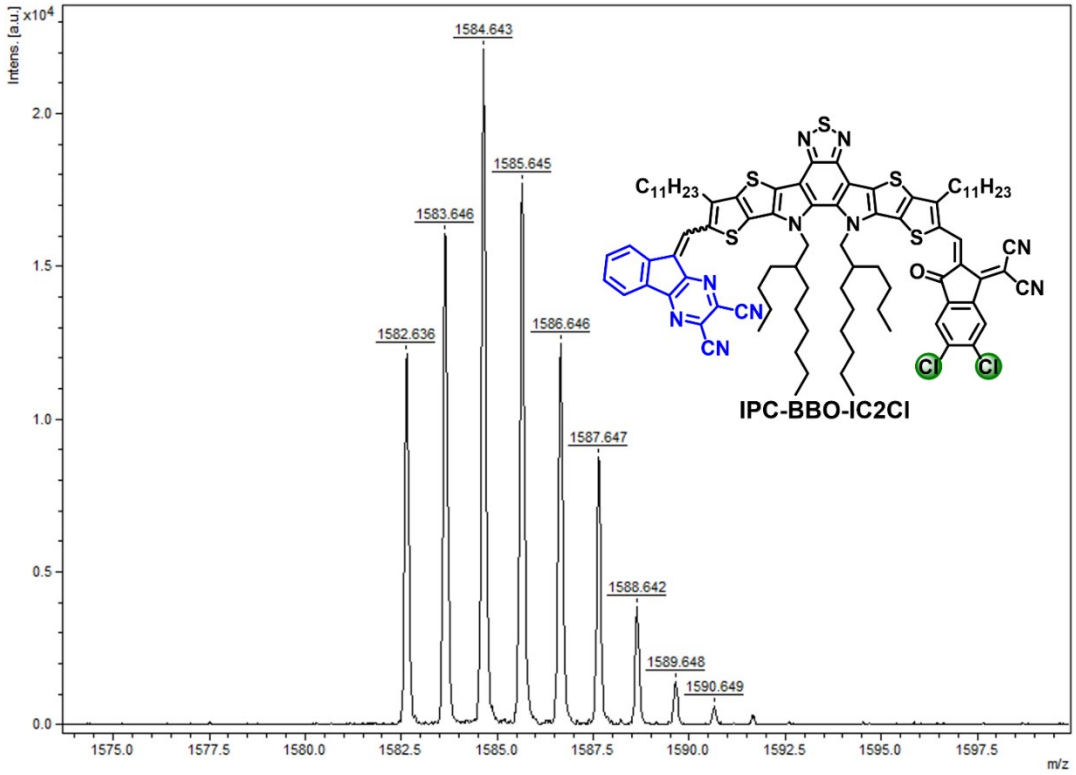

Fig. S14 Mass spectrum of IPC-BBO-IC2Cl by MALDI-TOF.

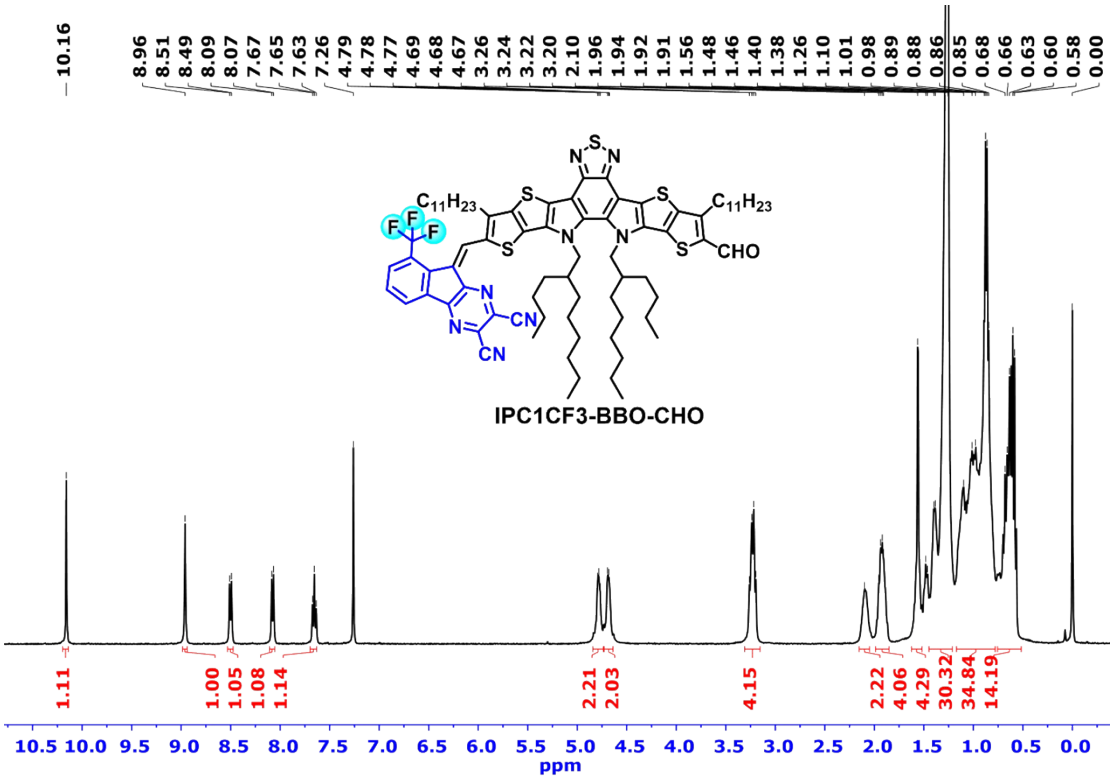

Fig. S15 ^{1}H NMR spectrum of IPC1CF3-BBO-CHO in $CDCl_3$.

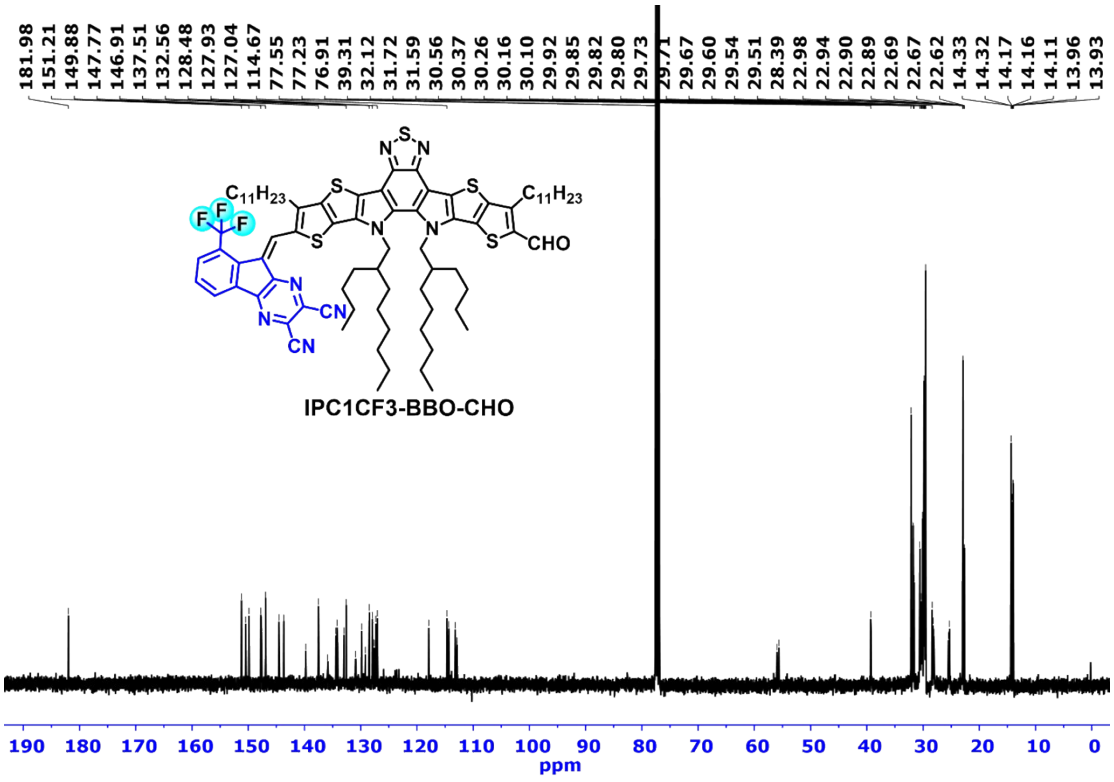

Fig. S16 ^{13}C NMR spectrum of IPC1CF3-BBO-CHO in $CDCl_3$.

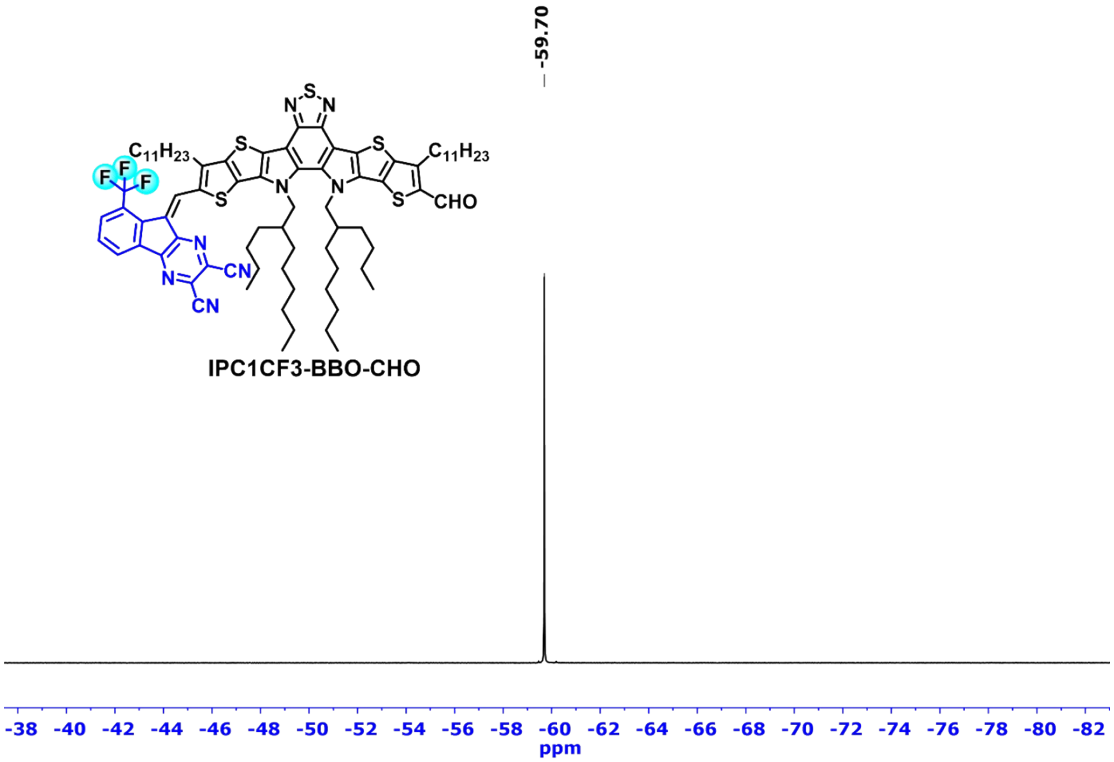

Fig. S17 ^{19}F NMR spectrum of IPC1CF3-BBO-CHO in $CDCl_3$.

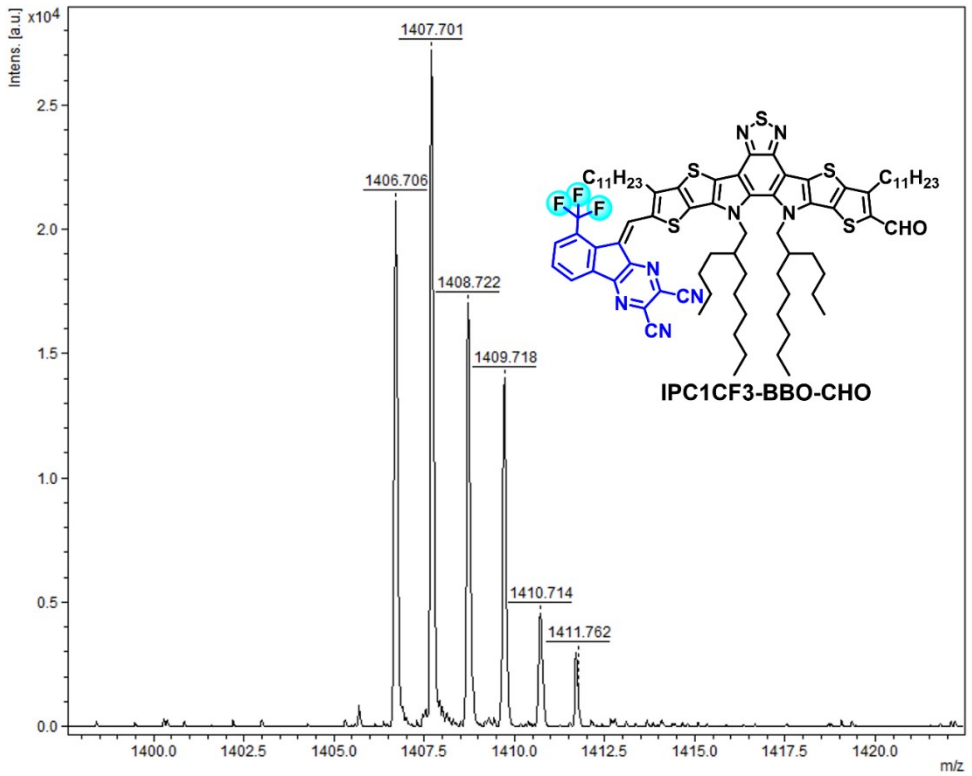

Fig. S18 Mass spectrum of IPC1CF3-BBO-CHO by MALDI-TOF.

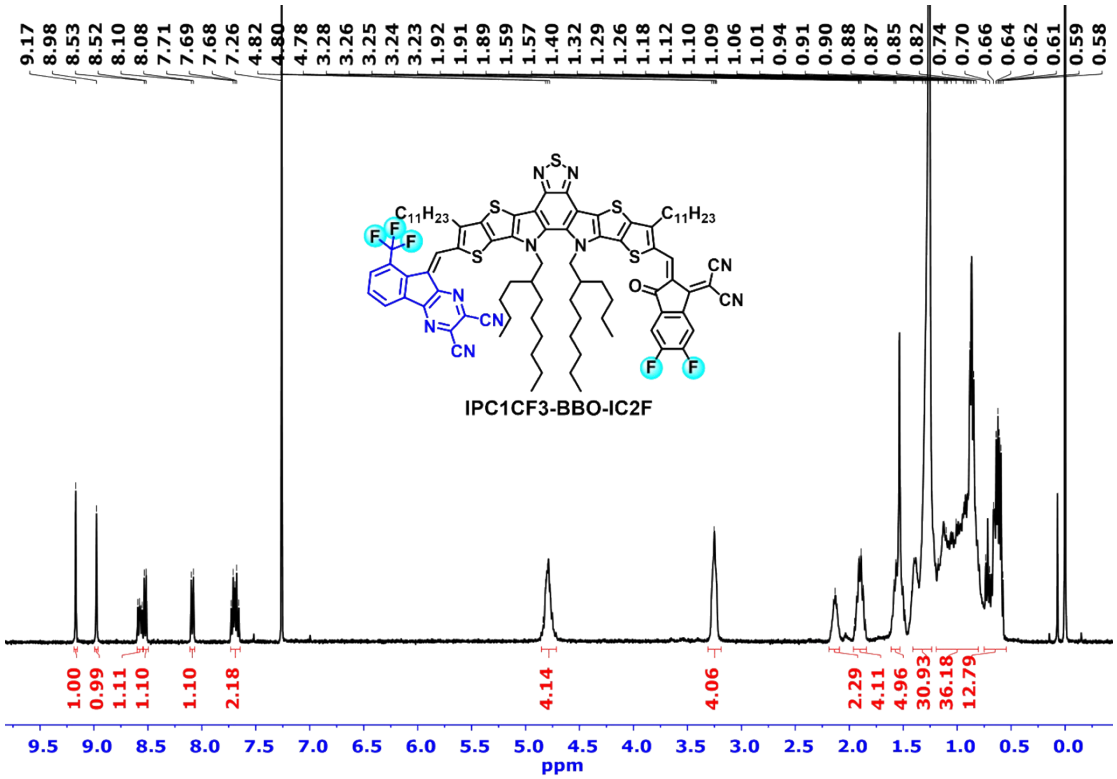

Fig. S19 ^{1}H NMR spectrum of IPC1CF3-BBO-IC2F in $CDCl_3$.

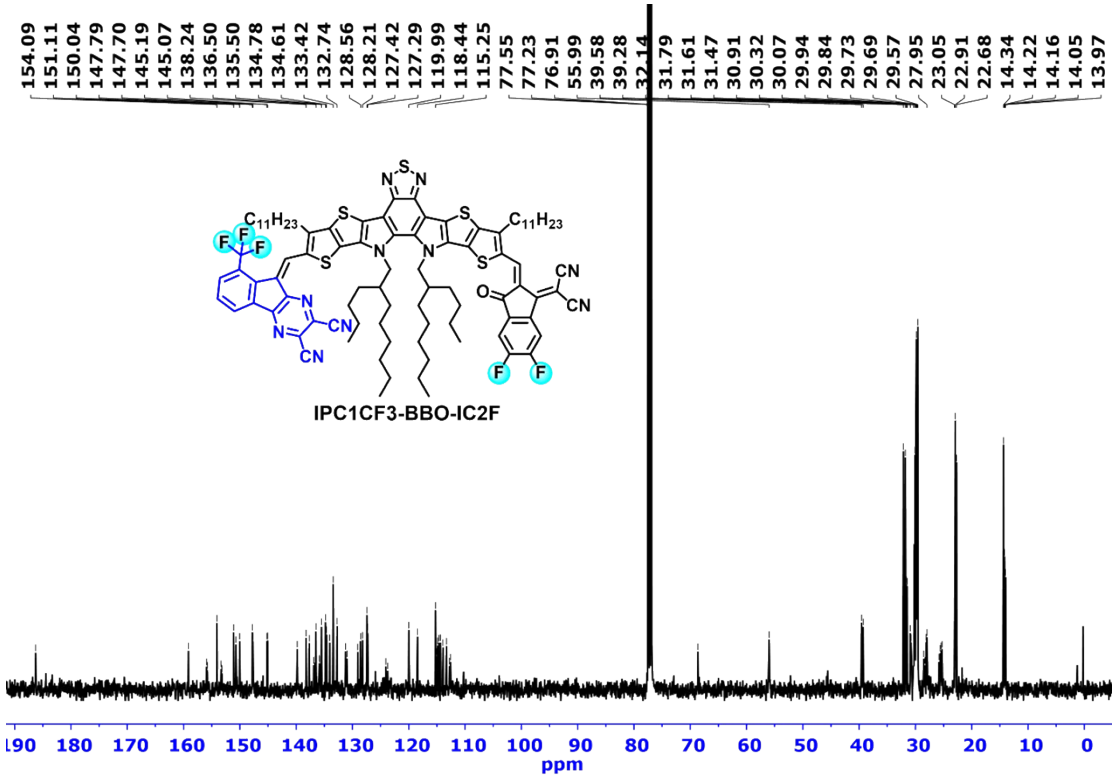

Fig. S20 ^{13}C NMR spectrum of IPC1CF3-BBO-IC2F in $CDCl_3$.

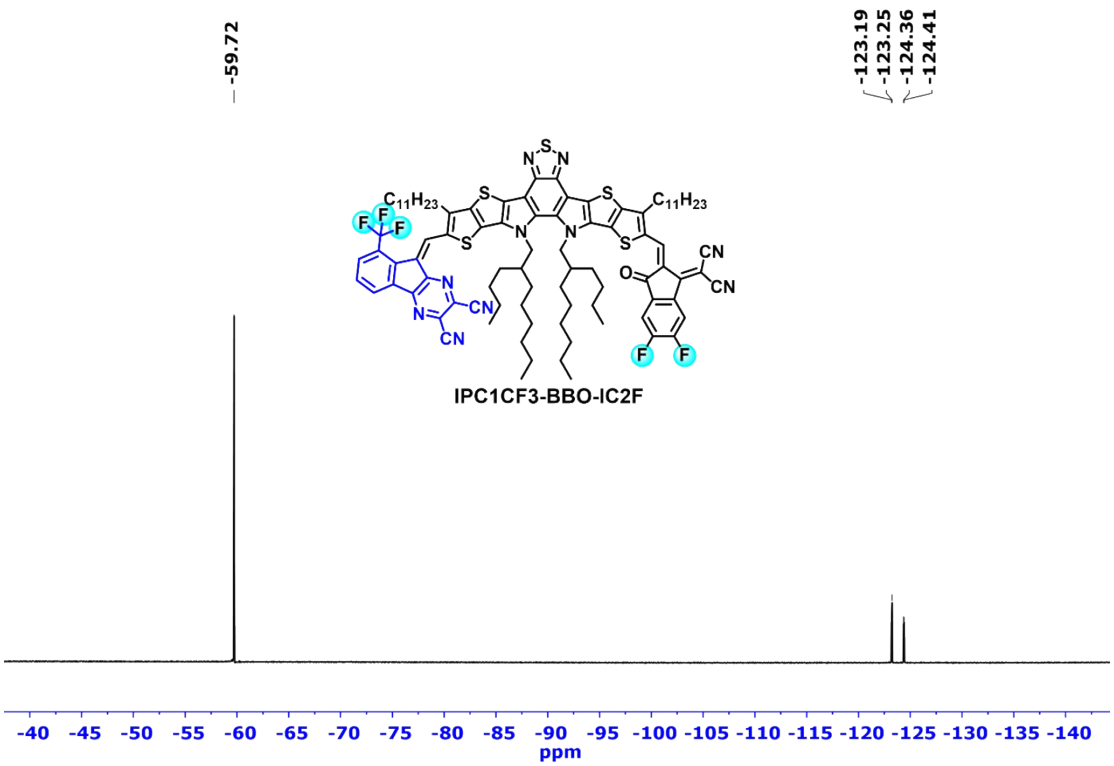

Fig. S21 ^{19}F NMR spectrum of IPC1CF3-BBO-IC2F in $CDCl_3$.

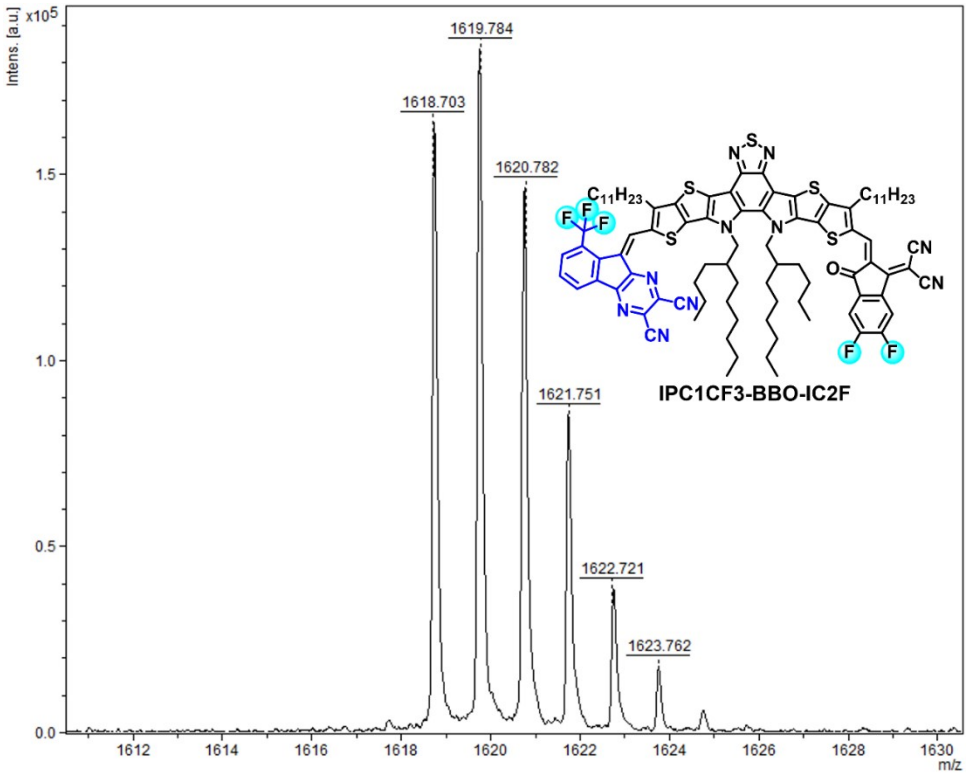

Fig. S22 Mass spectrum of IPC1CF3-BBO-IC2F using MALDI-TOF.

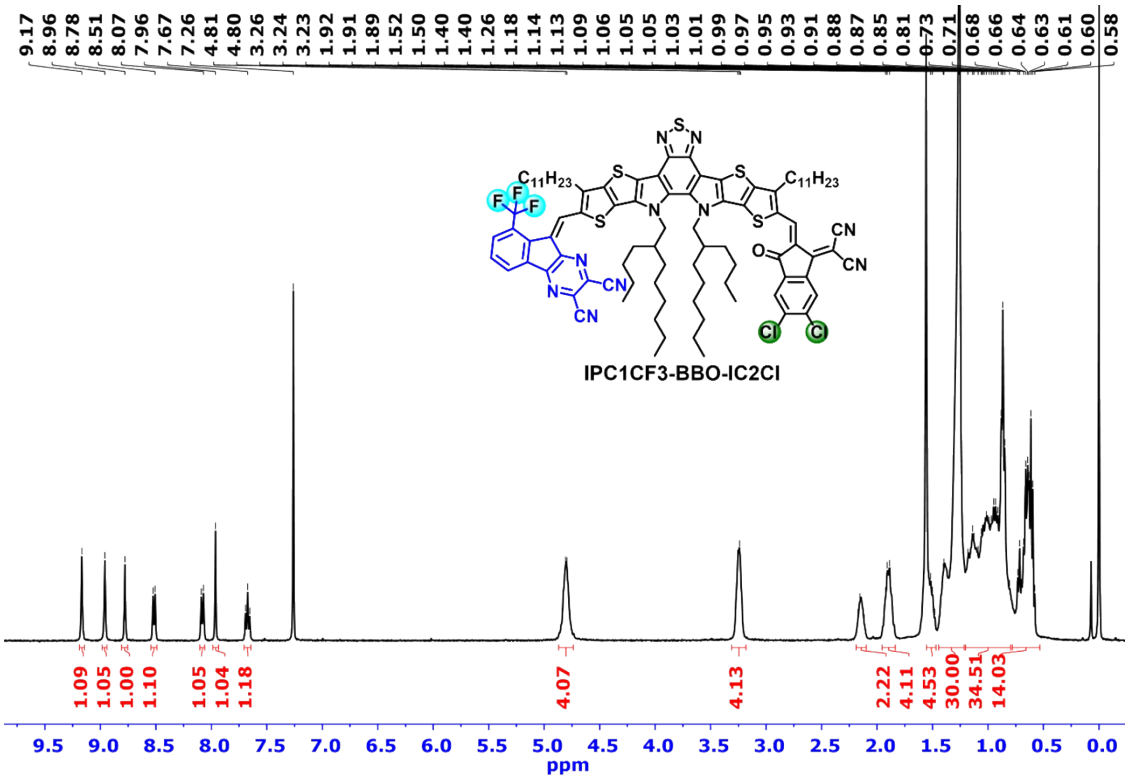

Fig. S23 ^{1}H NMR spectrum of IPC1CF3-BBO-IC2Cl in $CDCl_3$.

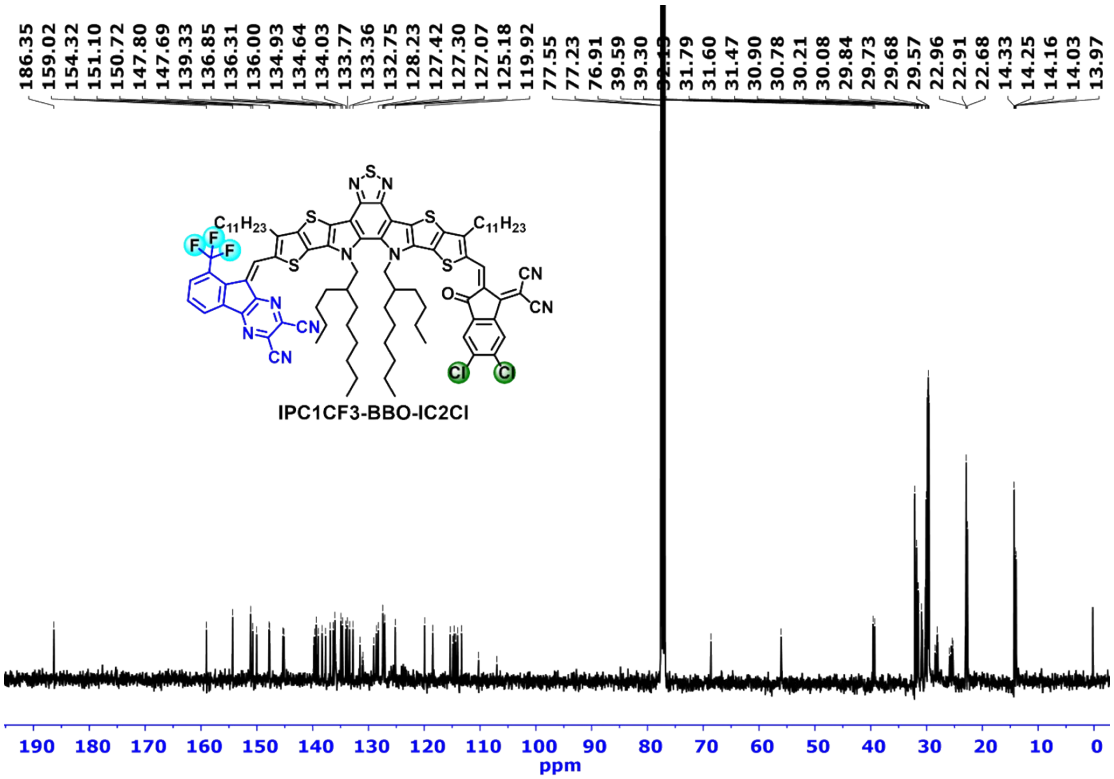

Fig. S24 ^{13}C NMR spectrum of IPC1CF3-BBO-IC2Cl in $CDCl_3$.

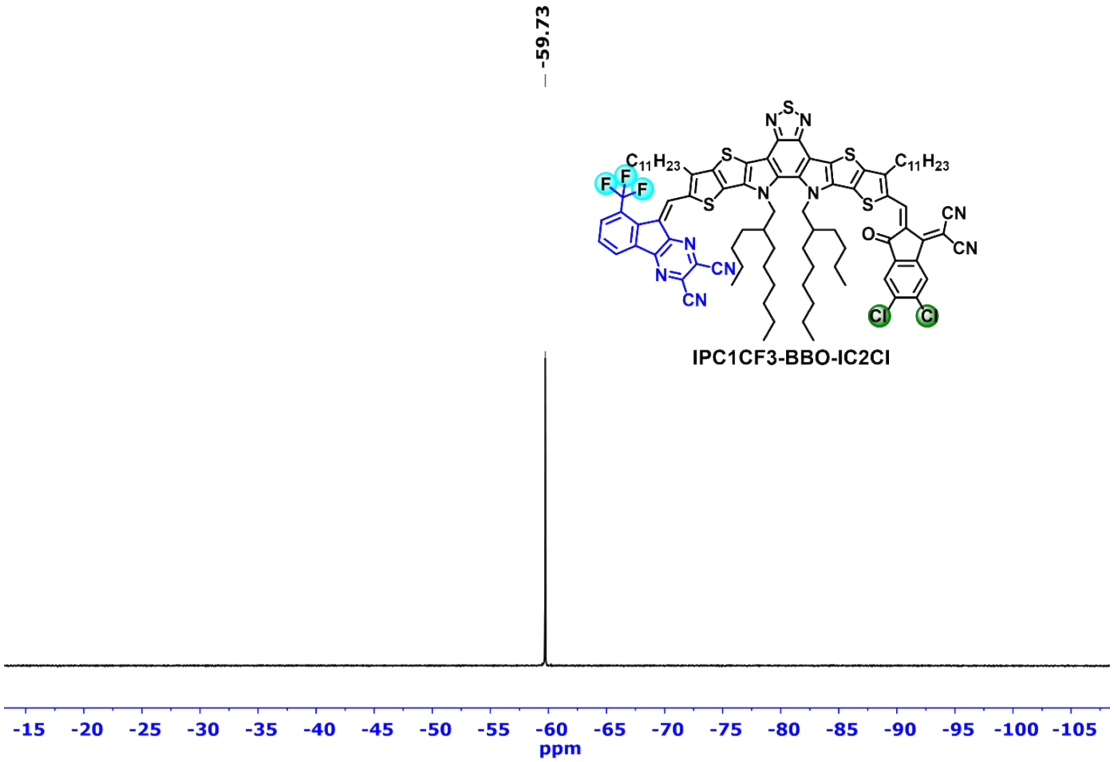

Fig. S25 ^{19}F NMR spectrum of IPC1CF3-BBO-IC2Cl in $CDCl_3$.

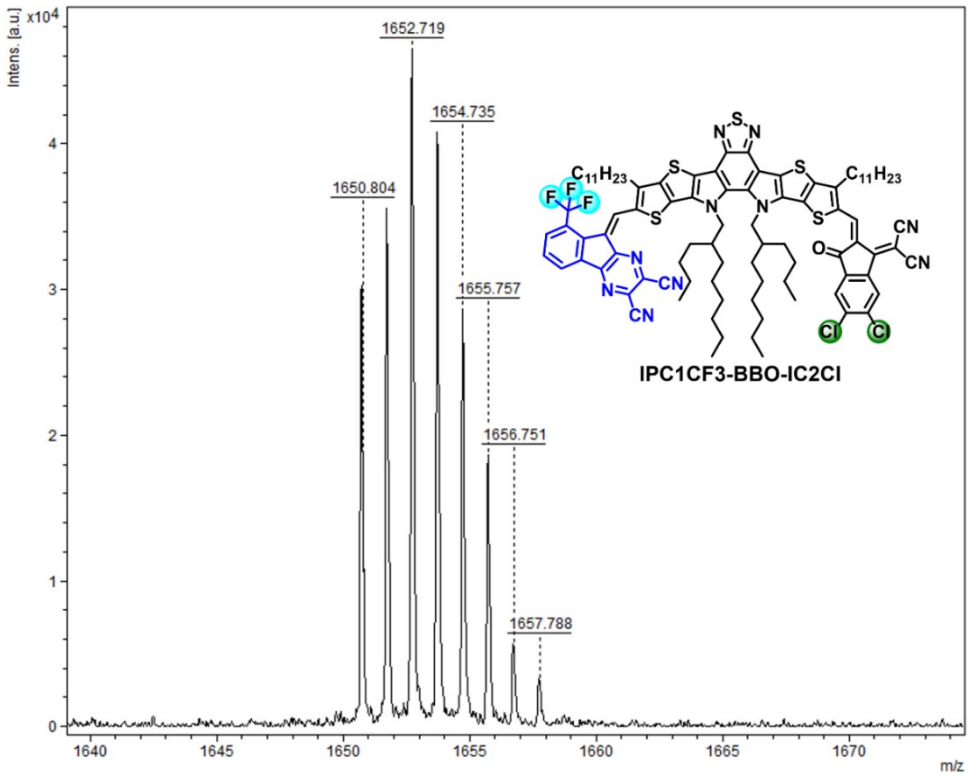

Fig. S26 Mass spectrum of IPC1CF3-BBO-IC2Cl using MALDI-TOF.

Results and Discussion_ Extended

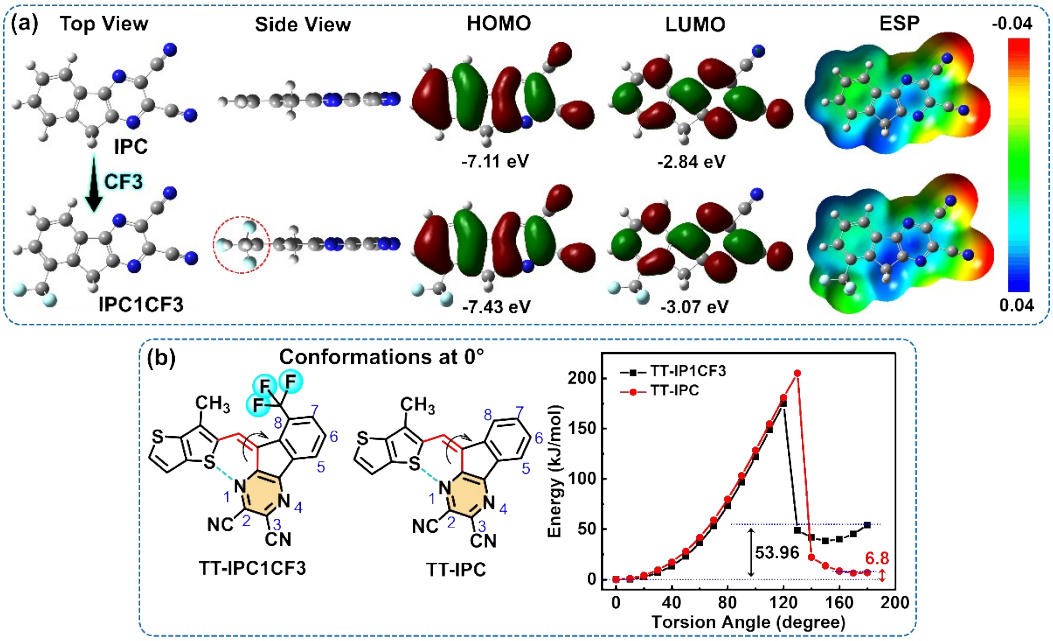

Fig. S27 (a) Optimized molecular structures, the HOMO and LUMO surface plots, and electrostatic potential surface diagrams of IPC and IPC1CF3. (b) Chemical structures and PES scan results of TT-IPC and TT-IPC1CF3.

To elucidate the molecular geometries and electronic structures of the end groups and NFAs, density functional theory (DFT) calculations at the B3LYP/6-31G(dp) level were performed using *Gaussian 09*. As shown in **Fig. S27a,** the optimized structures of both end groups preferentially adopt planar conformations due to their fused ring geometry. This, in turn, promotes efficient intermolecular π-π interactions through end-to-end stacking. However, the presence of the substantial CF3 group in IPC1CF3 (highlighted by the red circle in **Fig. S27a**) is expected to influence the intermolecular packing of the NFAs. The HOMO and LUMO energy levels of IPC1CF3 were significantly down-shifted from -7.11 to -7.43 eV and -2.84 to -3.07 eV, respectively, compared to IPC, due to the strong electron-withdrawing ability of the CF3 group. To assess the electron density distributions of the end groups, electrostatic potential surface (ESP) plots were analyzed based on their optimized geometries. As shown in **Fig. S27a**, red and blue colors represent the negative and positive electrostatic potential regions, respectively. Positive potential is distributed throughout the entire molecules in both IPC and IPC1CF3, while negative potential is located on the pyrazine nitrogen atoms and cyano groups. Additionally, negative

potential is observed on the CF3 group in IPC1CF3, indicating its strong electron-withdrawing ability. Relaxed potential energy surface (PES) scans were performed on model NFA molecules to identify their preferred conformations (**Fig. S27b**). Four types of PES scans were possible for these NFAs, involving single- and double-bond rotations between thieno[3,2-*b*]thiophene (TT) in the core and the end groups (IPC or IPC1CF3 and IC2F or IC2Cl). Our previous study demonstrated that for both rotations of TT-IC2F and the single bond rotation of TT-IPC, the conformers at 0° were the most stable.[1] However, in the case of double-bond rotation, TT-IPC exhibited two isomers at 0 and 180° with isomer ratios of 93.96 and 6.04%, respectively. To investigate the impact of the CF3 group on isomer formation, PES scans were performed for TT-IPC1CF3 by rotating a double bond, as shown in **Fig. S27b**. The optimized conformation of TT-IPC1CF3 was preferentially stable at 0°. This significant energy difference of 53.96 kJ/mol between the 0 and 180° isomers can be attributed to the steric hindrance between the TT and the CF3 group. The incorporation of the CF3 group at the eighth position of the IPC effectively restricted free rotation, resulting in the most stable conformation at 0°.

The molecular geometries of the NFAs were optimized by replacing the bulky alkyl chains with methyl groups to simplify the calculations using the preferred conformation of TT-IPC and the stable conformation of TT-IPC1CF3 as references. Theoretical calculations for IPC-BBO-IC2F are identical to those for IPC-BEH-IC2F because of their similar conjugated backbones.[1] The optimized geometries of the NFAs, including IPC-BBO-IC2F, exhibited nearly planar structures with small torsional angles between the core and end groups (**Fig. S28**). However, the angles between IPC and the core were found to be slightly smaller (0.07° for IPC-BBO-IC2F and 0.08° for IPC-BBO-IC2Cl) than those between IPC1CF3 and the core (0.22° for IPC1CF3-BBO-IC2F and 0.19° for IPC1CF3-BBO-IC2Cl), which was attributed to steric crowding of the CF3 group. These results indicate that NFAs with IPC1CF3 endings exhibit lower planarity than those with IPC endings. Notably, the CF3 group effectively controls isomer formation, as evidenced by the PES scans of their model compounds (**Fig. S27b**) and the H-NMR spectra of IPC-BBO-CHO and IPC1CF3-BBO-CHO (**Fig. S29**). The dipole moments of IPC1CF3-BBO-IC2F (11.31 D) and IPC1CF3-BBO-IC2Cl (12.07 D) were lower than those of IPC-BBO-IC2F (13.30 D) and IPC-BBO-IC2Cl (14.09 D). This difference is attributed to the CF3 group, which increases the electron density and reduces the positive charge in IPC1CF3. Overall, these findings indicate that

IPC1CF3-NFAs, with their reduced planarity and smaller dipole moments, are expected to exhibit

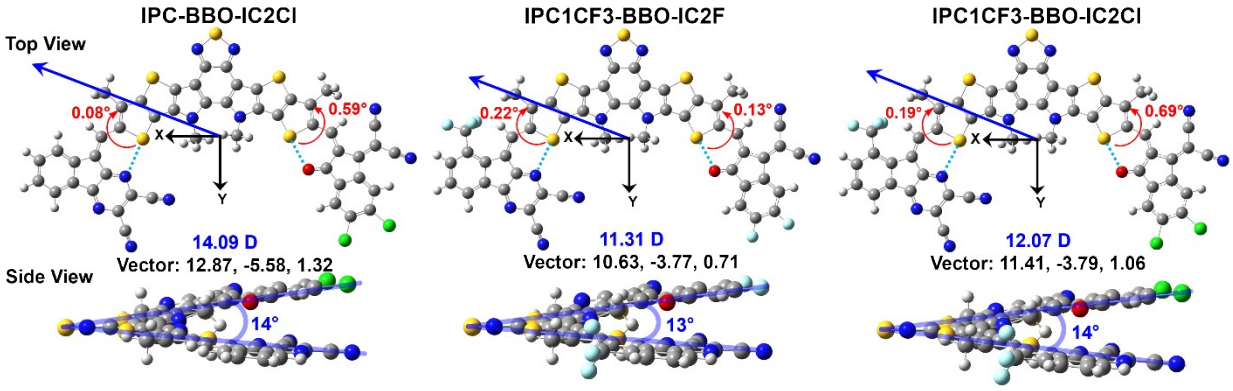

Fig. S28 Optimized molecular structures of NFAs.

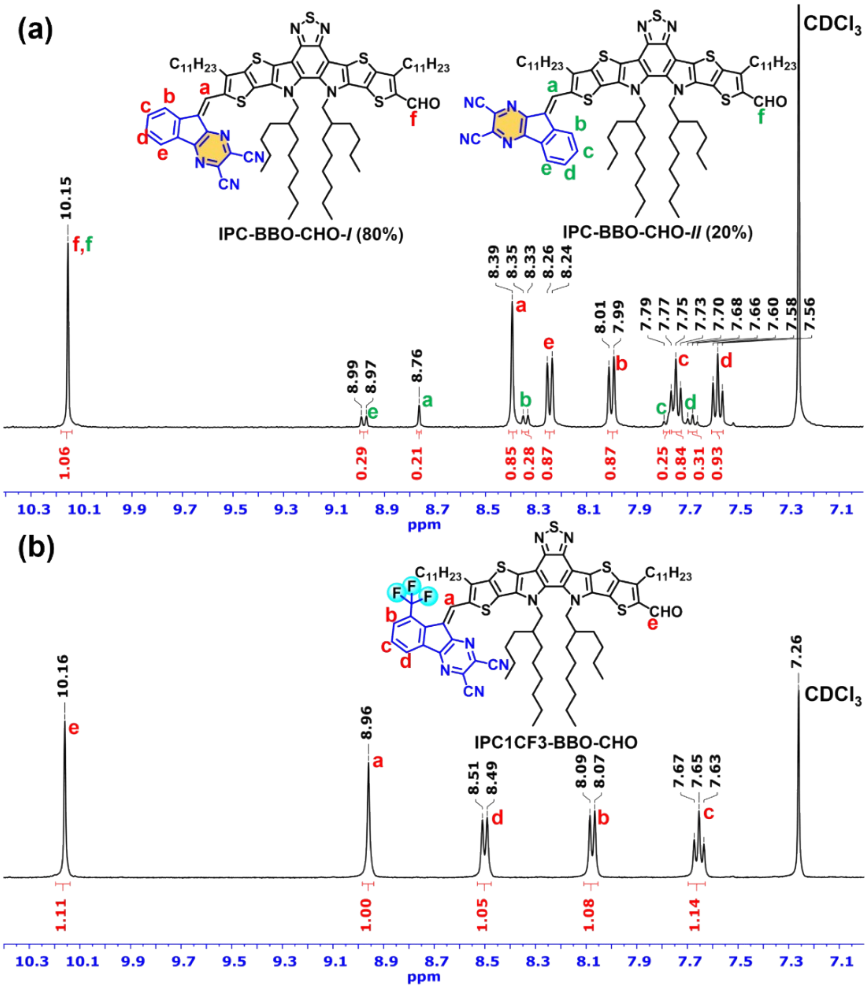

Fig. S29 Comparison of ^{1}H-NMR spectra of the aromatic regions of (a) IPC-BBO-CHO and (b) IPC1CF3-BBO-CHO.

weaker intermolecular π-π interactions, leading to diminished molecular aggregation compared with IPC-appended NFAs (IPC-NFAs).

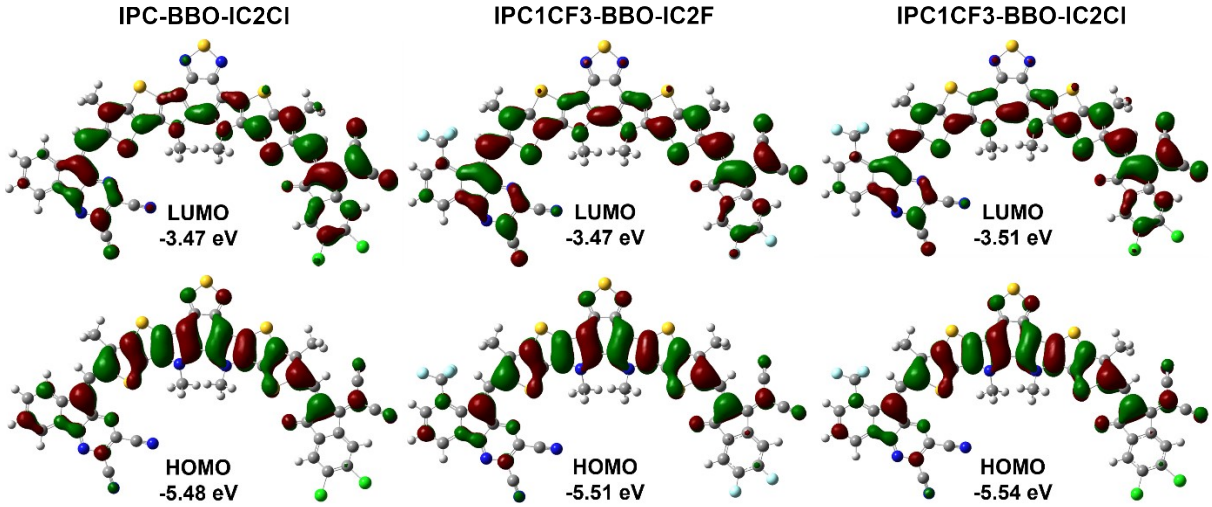

Fig. S30 HOMO and LUMO surface plots of IPC-BBO-IC2Cl, IPC1CF3-BBO-IC2F and IPC1CF3-BBO-IC2Cl.

The HOMO and LUMO surface plots of NFAs are depicted in **Fig. S30**. In the case of IPC-BBO-IC2F, these plots are identical to those of IPC-BEH-IC2F due to their similar conjugated backbones.[1] The HOMO was predominantly delocalized on the core, while the LUMO was mainly localized on the end groups. The HOMO/LUMO energy levels for IPC-BBO-IC2F, IPC-BBO-IC2Cl, IPC1CF3-BBO-IC2F and IPC1CF3-BBO-IC2Cl were calculated to be -5.45/-342, -5.48/-3.47, -5.51/-3.47, and -5.54/-3.51 eV, respectively. Owing to the strong electron-withdrawing ability of CF3 group, both IPC1CF3-based NFAs showed down-shifted energy levels compared to those of IPC-based NFAs. However, all NFAs exhibited an upshift compared to the energy levels of Y6, which were -5.61/-3.57 eV.[1] These results suggest that IPC and IPC1CF3 exhibit lower electron-withdrawing abilities than IC2F. Furthermore, replacing fluorine atoms with chlorine atoms on the IC moiety of IPC-BBO-IC2F and IPC1CF3-BBO-IC2F leads to deeper energy levels, attributed to the larger dipole moment of the carbon-chlorine bonds.

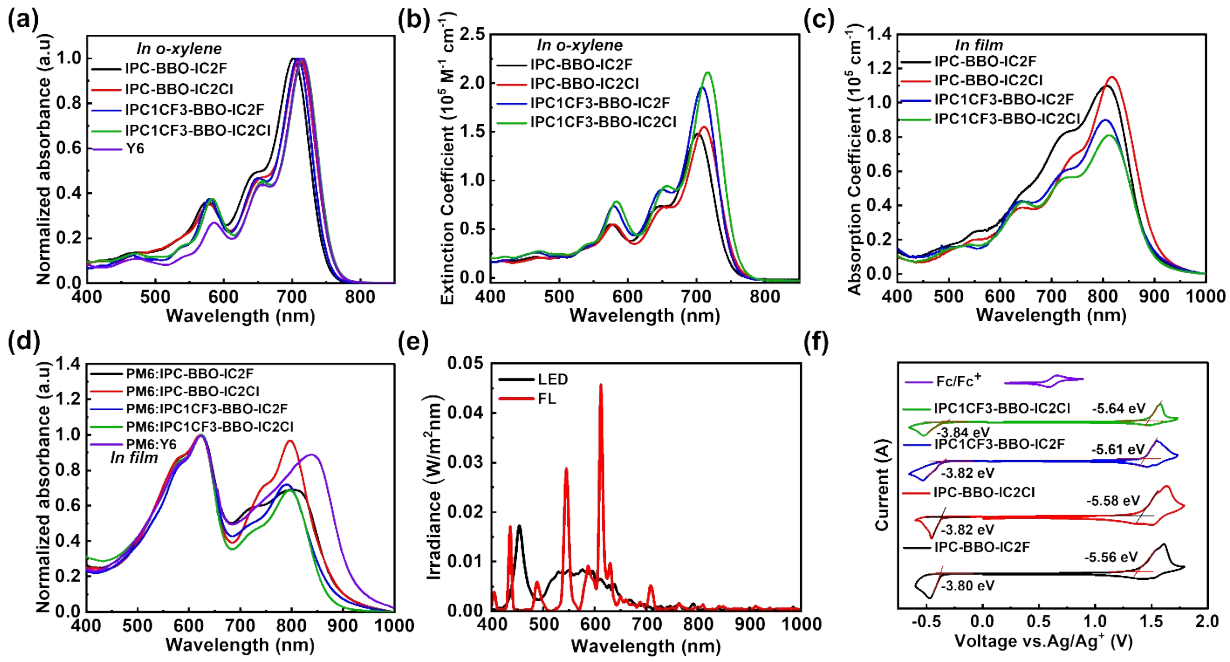

Fig. S31 UV-visible absorption spectra of NFAs in (a, b) *o*-xylene solutions and (c) film states. (d) UV-visible absorption spectra of blend films, (e) irradiation spectra of indoor light sources, and (f) cyclic voltammograms of NFAs.

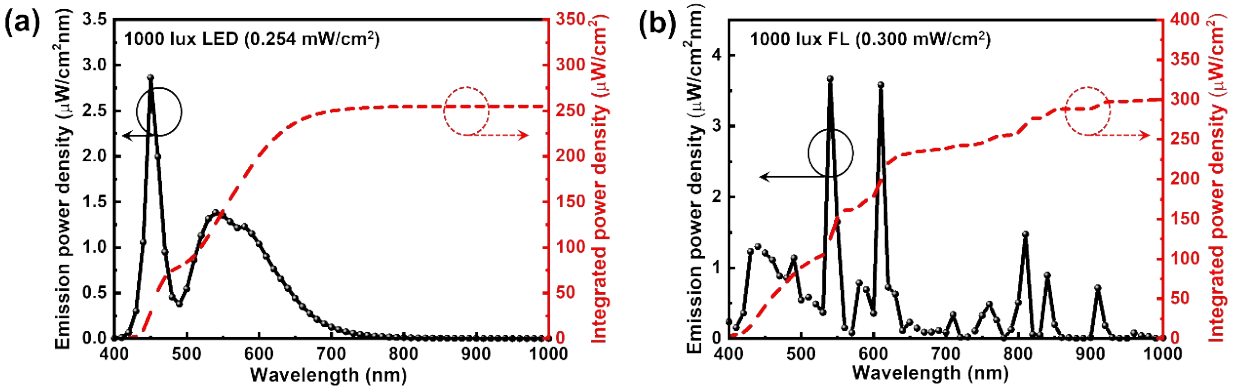

Fig. S32 Integrated emission power densities of (a) LED 1000 lux and (b) FL 1000 lux illumination.

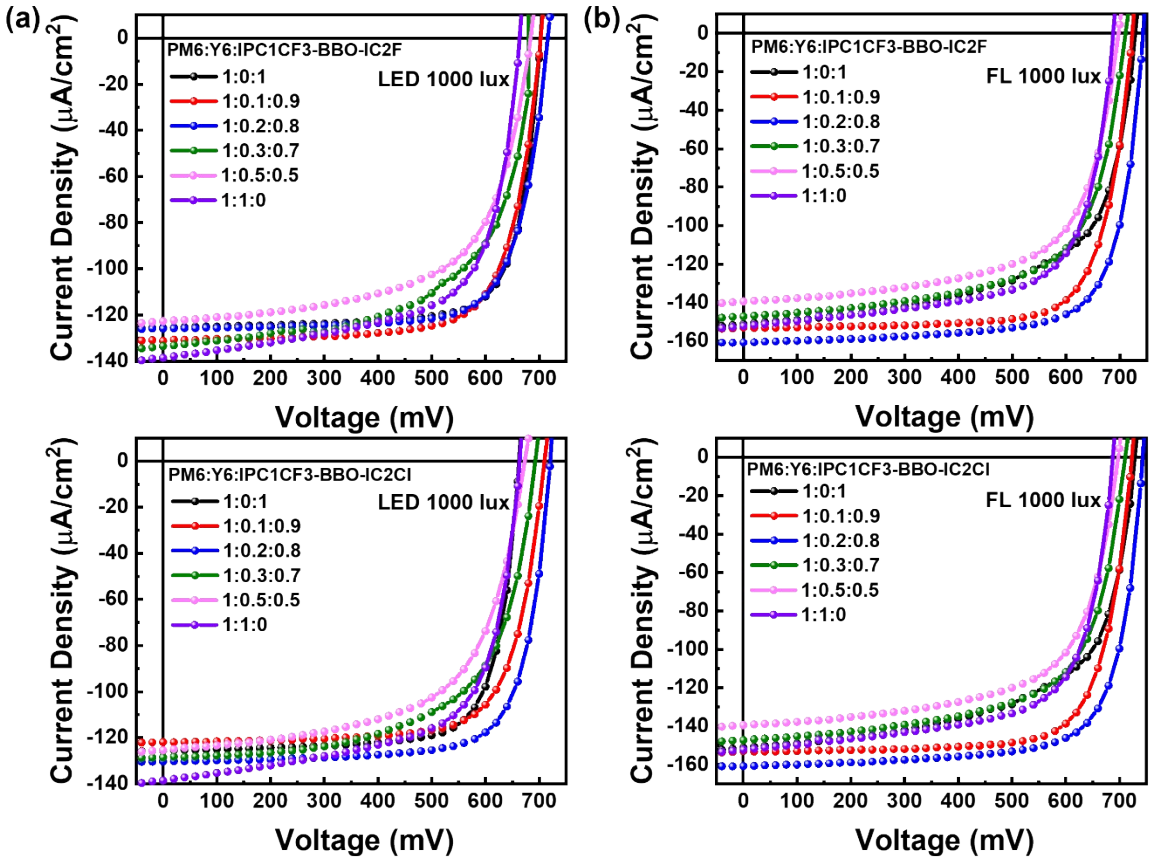

Fig. S33 *J-V* curves of the OPV devices with variable NFA ratios under (a) LED and (b) FL illumination.

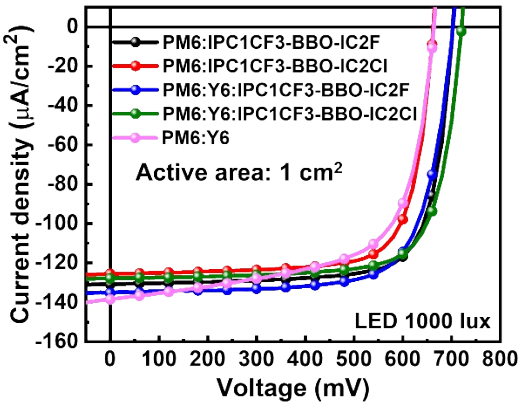

Fig. S34 *J-V* curves of large area (active area: 1 cm^2) OPV devices under 1000 lux LED illumination.

Table S1. Summary of photovoltaic parameters of OPV devices with variable NFA ratios under LED and FL illumination.

		PM6:Y6:IPC1CF3-BBO-IC2F				PM6:Y6:IPC1CF3-BBO-IC2Cl			
Light source	**Ratio**	**V_{OC} (mV)**	**J_{SC} (μA/cm²)**	**FF**	**PCE (%)**	**V_{OC} (mV)**	**J_{SC} (μA/cm²)**	**FF**	**PCE (%)**
LED 1000 lux	1.0:0:1.0	695 ± 3	129.1 ± 0.6	75.1 ± 0.3	26.5 ± 0.1	666 ± 5	124.5 ± 0.7	74.2 ± 0.9	24.1 ± 0.1
	1.0:0.1:0.9	702 ± 2	132.4 ± 2.6	73.3 ± 0.7	26.7 ± 0.1	709 ± 4	121.8 ± 1.2	73.5 ± 0.7	24.8 ± 0.1
	1.0:0.2:0.8	712 ± 3	129.7 ± 3.5	74.5 ± 0.3	26.9 ± 0.1	719 ± 2	128.1 ± 0.5	74.7 ± 0.7	27.0 ± 0.2
	1.0:0.3:0.7	680 ± 2	132.8 ± 1.0	62.5 ± 2.5	22.0 ± 0.2	692 ± 2	125.2 ± 0.9	64.2 ± 1.0	21.8 ± 0.2
	1.0:0.5:0.5	683 ± 2	126.3 ± 0.9	62.6 ± 1.1	21.2 ± 0.1	673 ± 4	122.7 ± 1.7	62.3 ± 1.9	20.1 ± 0.3
	1.0:1.0:0	662 ± 2	138.1 ± 2.6	69.1 ± 1.3	24.8 ± 0.2	662 ± 2	138.1 ± 2.6	69.1 ± 1.3	24.8 ± 0.2
FL 1000 lux	1.0:0:1.0	706 ± 2	161.8 ± 2.0	75.2 ± 0.4	28.4 ± 0.1	693 ± 2	153.8 ± 1.1	74.7 ± 0.3	26.4 ± 0.2
	1.0:0.1:0.9	723 ± 4	158.5 ± 1.2	71.3 ± 0.7	27.1 ± 0.2	728 ± 3	156.4 ± 1.0	75.3 ± 0.6	28.5 ± 0.1
	1.0:0.2:0.8	731 ± 3	165.5 ± 0.8	74.9 ± 0.3	30.1 ± 0.1	743 ± 2	158.6 ± 1.4	74.7 ± 0.5	29.2 ± 0.2
	1.0:0.3:0.7	665 ± 3	135.2 ± 4.5	55.5 ± 1.2	16.6 ± 0.2	710 ± 5	145.9 ± 3.5	65.2 ± 1.9	22.3 ± 0.2
	1.0:0.5:0.5	662 ± 2	128.4 ± 2.9	54.6 ± 0.9	15.4 ± 0.3	697 ± 3	139.2 ± 1.7	64.9 ± 2.2	20.9 ± 0.1
	1.0:1.0:0	671 ± 3	154.3 ± 1.0	66.8 ± 0.9	23.1 ± 0.1	671 ± 3	154.3 ± 1.0	66.8 ± 0.9	23.0 ± 0.1

Table S2. Summary of the photovoltaic parameters of reported indoor OPVs processed with non-halogenated solvents.

Photoactive layer	Processing solvent (Additive)	Light sources /Intensity	V_{OC} (mV)	J_{SC} (μA/cm²)	FF (%)	PCE (%)	Pout (μW/cm²)	Reference
PTQ10:tPDI2N-EH	Toluene (diphenyl ether)	LED/2000 lux	1070	139	48	11.7	71.4	3
PTB7-Th:PC71BM	*o*-xylene	LED/3000 lux	740	1022	62.0	14.3	469	4
PJ50:IT-4F6	Toluene	LED/500 lux	690	54.8	73	17.4	27.9	5
PV-X plus	*o*-xylene	LED/500 lux	670	53.3	77	19.3	-	6
PM6:ITIC-Th-s-m	*o*-xylene (1,8-octanedithiol)	LED/500 lux	860	39.1	72.0	22.5	39.2	7
J52-Cl:BTA3:BTA1	Tetrahydrofuran	LED/1000 lux	1120	96.7	80.0	28.8	86.9	8
PM6:Y6: IPC1CF3-BBO-IC2Cl	***o*-xylene**	**LED/1000 lux**	**719**	**128.1**	**74.7**	**27.1**	**68.8**	**This work**
PM6:Y6: IPC1CF3-BBO-IC2F	***o*-xylene**	**FL/1000 lux**	**731**	**165.5**	**74.9**	**30.2**	**90.6**	**This work**

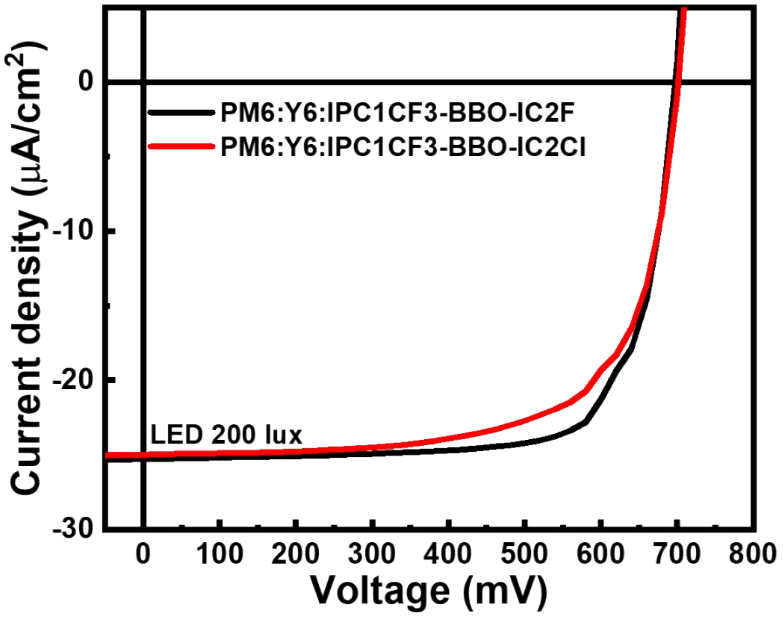

Fig. S35 *J-V* curves of PM6:Y6:IPC1CF3-BBO-IC2F and PM6:Y6:IPC1CF3-BBO-IC2Cl-based devices under 200 lux LED illumination.

Table S3. Summary of the photovoltaic parameters of PM6:Y6:IPC1CF3-BBO-IC2F and PM6:Y6:IPC1CF3-BBO-IC2Cl devices under LED illumination (200 lux).

Irradiance (P_{in}), luminescence (lux)	**Photoactive layer**	**V_{OC} (mV)**	**J_{SC} (μA/cm²)**	**FF (%)**	**PCE (%)**
0.065 mW/cm²	PM6:Y6:IPC1CF3-BBO-IC2F[a]	698 ± 2	24.8 ± 0.7	74.1 ± 0.9	19.8 ± 0.8
200	PM6:Y6:IPC1CF3-BBO-IC2Cl[a]	701 ± 1	24.4 ± 0.5	68.1 ± 0.5	18.0 ± 0.6

[a]Additive-free and *o*-xylene-processed OPVs

Table S4. Summary of the photovoltaic parameters of OPV devices under LED illumination (500 lux, 2000 lux).

Irradiance (P_{in}), luminescence (lux)	**Photoactive layer**	**V_{OC} (mV)**	**J_{SC} (μA/cm²)**	**FF (%)**	**PCE (%)**
0.138 mW/cm² 500	PM6:IPC-BBO-IC2F[a]	620 ± 8	35.5 ± 3.3	55.5 ± 1.1	8.8 ± 0.2
	PM6:IPC-BBO-IC2Cl[a]	670 ± 7	48.6 ± 2.5	56.3 ± 1.7	13.1 ± 0.3
	PM6:IPC1CF3-BBO-IC2F[a]	688 ± 4	68.4 ± 1.3	74.1 ± 0.8	25.3 ± 0.2
	PM6:IPC1CF3-BBO-IC2Cl[a]	662 ± 2	65.7 ± 0.9	73.6 ± 0.2	23.2 ± 0.2
	PM6:Y6:IPC1CF3-BBO-IC2F[a]	701 ± 2	72.5 ± 0.8	72.8 ± 1.3	26.8 ± 0.2
	PM6:Y6:IPC1CF3-BBO-IC2Cl[a]	693 ± 3	71.3 ± 1.0	73.7 ± 0.5	26.4 ± 0.1
	PM6:Y6[b]	638 ± 6	65.2 ± 1.3	70.6 ± 1.7	21.2 ± 0.2
0.506 mW/cm² 2000	PM6:IPC-BBO-IC2F[a]	655 ± 4	119.5 ± 2.0	54.9 ± 0.9	8.4 ± 0.4
	PM6:IPC-BBO-IC2Cl[a]	694 ± 5	150.1 ± 1.4	56.1 ± 1.0	11.7 ± 0.4
	PM6:IPC1CF3-BBO-IC2F[a]	716 ± 3	231.4 ± 0.7	73.6 ± 1.0	24.1 ± 0.1
	PM6:IPC1CF3-BBO-IC2Cl[a]	677 ± 4	228.4 ± 0.9	72.5 ± 2.4	22.2 ± 0.1
	PM6:Y6:IPC1CF3-BBO-IC2F[a]	718 ± 2	236.1 ± 1.0	72.9 ± 1.7	24.4 ± 0.2
	PM6:Y6:IPC1CF3-BBO-IC2Cl[a]	755 ± 3	238.3 ± 3.1	73.9 ± 1.9	26.3 ± 0.2
	PM6:Y6[b]	667 ± 2	229.8 ± 2.0	71.7 ± 0.5	21.7 ± 0.2

[a]Additive-free and *o*-xylene-processed OPVs. [b]CN (volume ratio:0.5%) and chloroform-processed OPVs.

Table S5. Photovoltaic parameters of OPV devices (active area: 1 cm^2) under 1000 lux LED illumination.

Photoactive layers	V_{OC} (mV)	J_{SC} (μA/cm^2)	FF (%)	PCE (%)
PM6:IPC1CF3-BBO-IC2F[a]	681	118.6	69.6	18.8
PM6:IPC1CF3-BBO-IC2Cl[a]	684	115.0	68.4	18.0
PM6:Y6:IPC1CF3-BBO-IC2F[a]	699	128.5	71.4	21.3
PM6:Y6:IPC1CF3-BBO-IC2Cl[a]	691	126.1	72.1	20.9
PM6:Y6[b]	689	122.4	65.5	18.3

[a]Additive-free and *o*-xylene-processed OPVs. [b]CN (volume ratio:0.5%) and chloroform-processed OPVs.

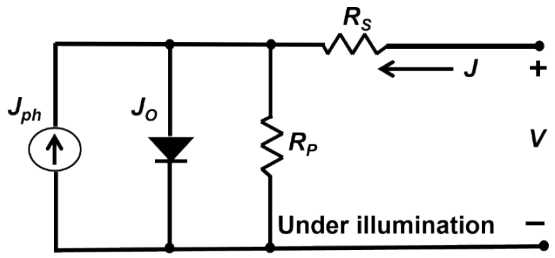

Fig. S36 Single-diode equivalent circuit model.

The OPV device characteristics can be characterized using a single-diode equivalent circuit model under illumination, which consists of one current source and two parasitic resistances, namely, the R_P and R_S. R_P is associated with factors such as leakage current and recombination, whereas R_S originates from the resistive elements within the device, including the electrode resistance and bulk resistance in the photoactive layers.[9]

The FF evolution can be understood within the framework of an equivalent circuit model. FF, defined as $(J_{max} \times V_{max})/(J_{SC} \times V_{OC})$, can be demonstrated to be a function of the normalized open-circuit voltage ($v_{OC} = eV_{OC}/nkT$), normalized series resistance ($r_S = R_S/R_{CH}$), and normalized shunt resistance ($r_P = R_P/R_{CH}$). Here, the characteristic resistance (R_{CH}) is given by $R_{CH} = V_{OC}/J_{SC}$ and by

considering the effects of R_S and R_P, a semi-empirical equation for FF can be derived.[10]

$$FF = \left\{\frac{v_{OC} - ln(v_{OC} + 0.72)}{(v_{OC} + 1)}\right\}(1 - 1.1r_s) + 0.19{r_s}^2\left\{1 - \frac{(v_{OC} + 0.7)\left\{\frac{v_{OC} - ln(v_{OC} + 0.72)}{v_{OC} + 1}\right\}(1 - 1.1r_s) + 0.19{r_s}^2}{v_{OC} \qquad r_P}\right\}$$

$(0 < r_s + 1/r_P < 0.4)$

Table S6. Summary of the parasitic resistances of the OPV devices under different light sources.

Light sources	Photoactive layers	R_P (Ω.cm²) ×10⁵	R_S (Ω.cm²) ×10²	r_S	r_P
LED 1000 lux	PM6:IPC-BBO-IC2F	2.17	78.6	0.802	22.2
	PM6:IPC-BBO-IC2Cl	1.15	53.0	0.716	15.4
	PM6:IPC1CF3-BBO-IC2F	3.49	6.98	0.129	64.9
	PM6:IPC1CF3-BBO-IC2Cl	2.39	6.35	0.118	44.8
	PM6:Y6:IPC1CF3-BBO-IC2F	3.39	6.75	0.123	61.9
	PM6:Y6:IPC1CF3-BBO-IC2Cl	2.47	7.45	0.128	42.5
	PM6:Y6	1.73	6.61	0.137	36.2
FL 1000 lux	PM6:IPC-BBO-IC2F	2.12	78.4	0.745	20.2
	PM6:IPC-BBO-IC2Cl	1.23	33.9	0.454	16.5
	PM6:IPC1CF3-BBO-IC2F	1.83	7.56	0.173	42.0
	PM6:IPC1CF3-BBO-IC2Cl	2.15	4.35	0.096	47.7
	PM6:Y6:IPC1CF3-BBO-IC2F	1.67	6.38	0.144	37.8
	PM6:Y6:IPC1CF3-BBO-IC2Cl	2.28	5.05	0.108	49.1
	PM6:Y6	2.00	4.98	0.114	46.0

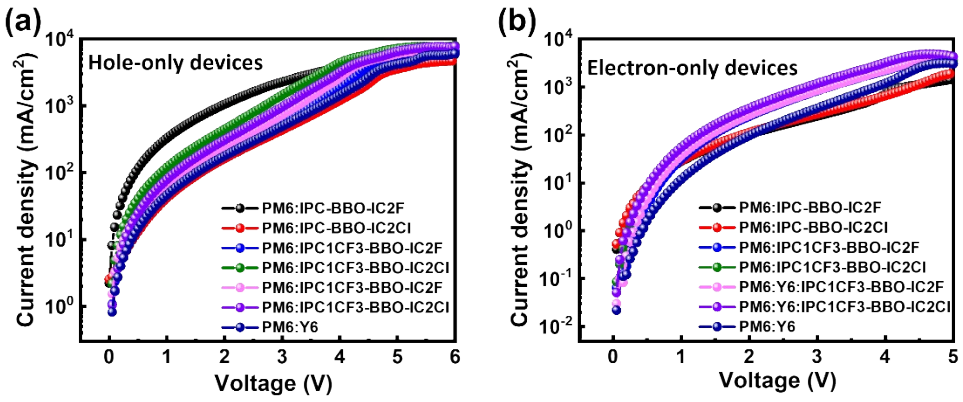

Fig. S37 *J-V* curves of the (a) hole-only and (b) electron-only devices.

Table S7. Hole and electron mobilities as measured in hole-only and electron-only devices.

Photoactive layer	Hole mobility ($cm^2 V^{-1} s^{-1}$)	Electron mobility ($cm^2 V^{-1} s^{-1}$)	μ_e/μ_h
PM6:IPC-BBO-IC2F	1.23×10^{-3}	0.26×10^{-3}	0.211
PM6:IPC-BBO-IC2Cl	1.04×10^{-3}	0.41×10^{-3}	0.394
PM6:IPC1CF3-BBO-IC2F	1.30×10^{-3}	1.21×10^{-3}	0.928
PM6:IPC1CF3-BBO-IC2Cl	1.22×10^{-3}	1.13×10^{-3}	0.936
PM6:Y6:IPC1CF3-BBO-IC2F	1.55×10^{-3}	1.50×10^{-3}	0.969
PM6:Y6:IPC1CF3-BBO-IC2Cl	1.60×10^{-3}	1.69×10^{-3}	1.053
PM6:Y6	0.98×10^{-3}	1.22×10^{-3}	1.246

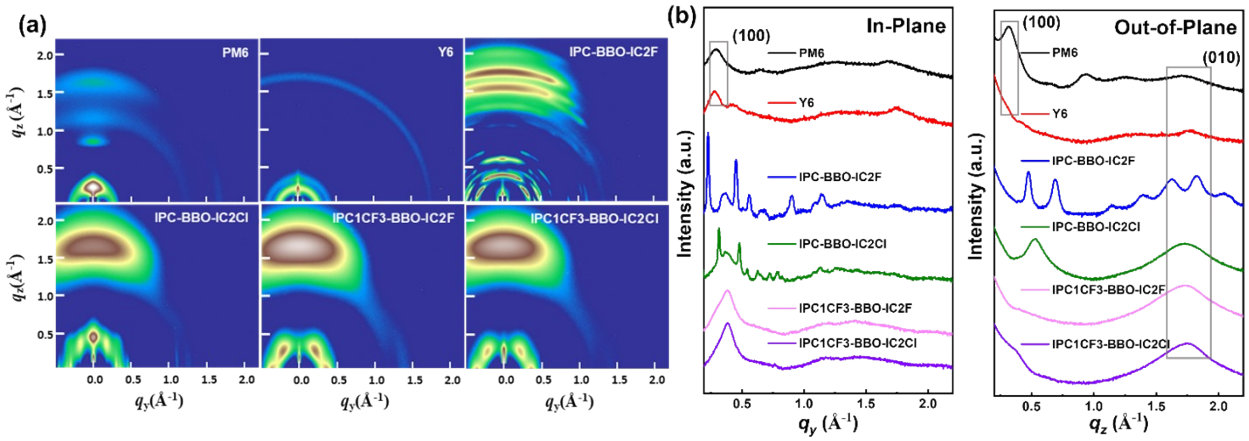

Fig. S38 (a) GIWAXS diffraction patterns and (b) Line-cut profiles of neat PM6 and NFAs films in the in-plane (IP) and in the out-of-plane (OOP) directions.

Table S8. Summary of GIWAXS parameters for neat films of PM6 and NFAs.

Neat films	In-Plane				Out-of-Plane							
	Lamellar stacking				Lamellar stacking				π-π stacking			
	(100)				(300)				(010)			
	q (Å^{-1})	*d* (Å)	Height (a.u.)	CCL (nm)	*q* (Å^{-1})	*d* (Å)	Height (a.u.)	CCL (nm)	*q* (Å^{-1})	*d* (Å)	Height (a.u.)	CCL (nm)
PM6	0.290	21.65	445	5.10	0.937	6.71	223	4.12	1.704	3.69	213	1.48
Y6	0.278	22.60	295	29.7	-	-	-	-	1.766	3.56	75.6	2.17
IPC-BBO-IC2F	-	-	-	-	-	-	-	-	1.625 1.825	3.87 3.44	753 965	5.17 6.57
IPC-BBO-IC2Cl	-	-	-	-	-	-	-	-	1.732	3.63	1636	1.77
IPC1CF3-BBO-IC2F	-	-	-	-	-	-	-	-	1.735	3.62	3374	1.98
IPC1CF3-BBO-IC2Cl	-	-	-	-	-	-	-	-	1.738	3.62	1689	2.68
Blend films	**In-Plane**				**Out-of-Plane**							
	Lamellar stacking				**Lamellar stacking**				**π-π stacking**			
	$(100)_p$				**$(300)_p$**				**(010)**			
	q (Å^{-1})	***d*** (Å)	**Height (a.u.)**	**CCL (nm)**	***q*** (Å^{-1})	***d*** (Å)	**Height (a.u.)**	**CCL (nm)**	***q*** (Å^{-1})	***d*** (Å)	**Height (a.u.)**	**CCL (nm)**
PM6:IPC-BBO-IC2F	0.293	2141	1142	6.34	0.934	6.73	150	4.72	1.634 1.821	3.85 3.45	1214 1392	3.68 5.46
PM6:IPC-BBO-IC2Cl	0.304	20.65	1074	6.02	0.924	6.80	145	5.09	1.717	3.66	1109	1.85
PM6:IPC1CF3-BBO-IC2F	0.297	21.13	1628	8.26	0.919	6.84	79.2	6.45	1.733	3.63	1179	2.09
PM6:IPC1CF3-BBO-IC2Cl	0.297	21.18	1372	8.06	0.924	6.80	59.1	7.96	1.732	3.63	1190	2.00
PM6:Y6:IPC1CF3-BBO-IC2F	0.297	21.15	1274	8.42	0.919	6.84	58.1	7.38	1.737	3.62	822	2.18
PM6:Y6:IPC1CF3-BBO-IC2Cl	0.296	21.25	1428	7.87	0.930	6.79	41.8	7.25	1.735	3.62	1083	2.30

References in Supporting Information

1. P. Gopikrishna, H. Choi, D. H. Kim, J. H. Hwang, Y. Lee, H. Jung, G. Yu, T. B. Raju, E. Lee, Y. Lee, S. Cho and B. Kim, *Chem. Sci.,* 2021, **12**, 14083-14097.
2. P. Gopikrishna, H. Choi, D. H. Kim, D. Lee, J. H. Hwang, S-M. Jin, E Lee, S. Cho and B. Kim, *Small* 2024, **20**, 2401080.
3. F. Tintori, A. Laventure, J. D. Koenig and G. C. Welch, *J. Mater. Chem. C* 2020, **8**, 13430-13438.
4. M. Cui, A. Lv and Z. Ma, *ChemPhysChem* 2022, **23**, e202200091.
5. S. H. Park, N. Y. Kwon, H. J. Kim, E. Cho, H. Kang, A. K. Harit, H. Y. Woo, H. J. Yoon, M.J. Cho, D. H. Choi, *ACS Appl. Mater. Interfaces* 2021, **13**, 13487-13498.
6. D. Müller, L. Campos Guzmán, E. Jiang, B. Zimmermann and U. Würfel, *Solar RRL* 2022, **6,** 2200175.
7. N.G. An, J. E. Lee, W. Lee, D. Yuk, S. Song, C. Wang, S.-K. Kwon, Y.-H. Kim and J. Y. Kim, *J. Mater. Chem. C* 2022, **10**, 15781-15791.
8. Q. Wu, Y. Yu, X. Xia, Y. Gao, T. Wang, R. Sun, J. Guo, S. Wang, G. Xie, X. Lu, E. Zhou and J. Min, *Joule* 2022, **6**, 2138-2151.
9. J. D. Servaites, M. A. Ratner and T. J. Marks, *Energy Environ. Sci.*, 2011, **4**, 4410-4422.
10. J. S. Goo, J.-H. Lee, S.-C. Shin, J.-S. Park and J. W. Shim, *J. Mater. Chem. A* 2018, **6**, 23464-23472.